Flecker, R., Ducassou, E., Williams, T., and the Expedition 401 Scientists
Proceedings of the International Ocean Discovery Program Volume 401
publications.iodp.org

Expedition 401 summary[1]

R. Flecker, E. Ducassou, T. Williams, U. Amarathunga, B. Balestra, M.A. Berke, C.L. Blättler, S. Chin, M. Das, K. Egawa, N. Fabregas, S.J. Feakins, S.C. George, F.J. Hernández-Molina, W. Krijgsman, Z. Li, J. Liu, D. Noto, F. Raad, F.J. Rodríguez-Tovar, F.J. Sierro, P. Standring, J. Stine, E. Tanaka, M. Teixeira, X. Xu, S. Yin, and M.Z. Yousfi[2]

[1] Flecker, R., Ducassou, E., Williams, T., Amarathunga, U., Balestra, B., Berke, M.A., Blättler, C.L., Chin, S., Das, M., Egawa, K., Fabregas, N., Feakins, S.J., George, S.C., Hernández-Molina, F.J., Krijgsman, W., Li, Z., Liu, J., Noto, D., Raad, F., Rodríguez-Tovar, F.J., Sierro, F.J., Standring, P., Stine, J., Tanaka, E., Teixeira, M., Xu, X., Yin, S., and Yousfi, M.Z., 2025. Expedition 401 summary. In Flecker, R., Ducassou, E., Williams, T., and the Expedition 401 Scientists, Mediterranean–Atlantic Gateway Exchange. Proceedings of the International Ocean Discovery Program, 401: College Station, TX (International Ocean Discovery Program). https://doi.org/10.14379/iodp.proc.401.101.2025
[2] **Expedition 401 Scientists' affiliations.**

Contents

Keywords
International Ocean Discovery Program, IODP, *JOIDES Resolution*, Expedition 401, Mediterranean–Atlantic Gateway Exchange, Earth Systems Models, Site U1609, Site U1610, Site U1385, Site U1611, IMMAGE, Land-2-Sea, Gibraltar, Messinian Salinity Crisis, Messinian, Tortonian, Miocene, Pliocene, contourite, turbidite, slump, debrite, hemipelagite, cemented carbonate, sapropel, organic-rich mud, sandstone, drift, mixed system, Mediterranean Overflow Water, MOW, Mediterranean, outflow, salt giant, evaporite, gypsum, halite, precession, Atlantic, exchange, Portuguese margin, Gulf of Cádiz, Alborán Basin, Sines drift

Core descriptions

Supplementary material

References (RIS)

MS 401-101
Published 7 July 2025

Funded by NSF OCE1326927, ECORD, and JAMSTEC

Abstract

Marine gateways play a critical role in the exchange of water, heat, salt, and nutrients between oceans and seas. Changes in gateway geometry can significantly alter both the pattern of global ocean circulation and climate. Today, the volume of dense water supplied by Atlantic–Mediterranean exchange through the Gibraltar Strait is among the largest in the global ocean. For the past 5 My, this overflow has generated a saline plume at intermediate depths in the Atlantic that deposits distinctive contouritic sediments and contributes to the formation of North Atlantic Deep Water. This single gateway configuration only developed in the Early Pliocene. During the Miocene, two narrow corridors linked the Mediterranean and Atlantic: one in northern Morocco and the other in southern Spain. Progressive restriction and closure of these corridors resulted in extreme salinity fluctuations in the Mediterranean and the precipitation of the Messinian Salinity Crisis salt giant. International Ocean Discovery Program (IODP) Expedition 401 is the offshore drilling component of a Land-2-Sea drilling proposal, Investigating Miocene Mediterranean–Atlantic Gateway Exchange (IMMAGE). Its aim is to recover a complete record of Atlantic–Mediterranean exchange from its Late Miocene inception to its current configuration by targeting Miocene offshore sediments on either side of the Gibraltar Strait. Miocene cores from the two precursor connections now exposed on land will be obtained by future International Continental Scientific Drilling Program (ICDP) campaigns.

Plain language summary

Today, Mediterranean–Atlantic seawater exchange takes place exclusively through the Gibraltar Strait. Around 8 million years ago, however, there were another two gateways: one in northern Morocco and the other through southern Spain. Both connections have subsequently closed and been tectonically uplifted and preserved on land. Extreme narrowing of these pre-Gibraltar Strait connections raised salinity in the Mediterranean substantially, leading to the precipitation of more than 1 km of salt on the Mediterranean's seafloor, termed the "salt giant." This process may have contributed to a major episode of global cooling. The chemical and physical properties of the sediments preserved in and on either side of these corridors are key to understanding and quantifying this global cooling. International Ocean Discovery Program (IODP) Expedition 401 is the offshore drilling component of a Land-2-Sea drilling proposal, Investigating Miocene Mediterranean–Atlantic Gateway Exchange (IMMAGE). Records of exchange preserved off shore in the Atlantic and Mediterranean were recovered during Expedition 401. Future onshore drilling will target the fossil gateway records that are now preserved on land.

1. Introduction

Marine gateways play a critical role in the exchange of water, heat, salt, and nutrients between oceans and seas. The advection of dense waters helps drive global thermohaline circulation, and because the ocean is the largest of the rapidly exchanging CO_2 reservoirs, this advection also affects atmospheric carbon concentration. Changes in gateway geometry can therefore significantly alter both the pattern of global ocean circulation and associated heat transport and climate, as well as having a profound local impact. Today, the volume of dense water supplied by Atlantic–Mediterranean exchange through the Gibraltar Strait is among the largest in the global ocean (Figure **F1**). For the past 5 My, this overflow has generated a saline plume at intermediate depths in the Atlantic that deposits distinctive contouritic sediments in the Gulf of Cádiz and contributes to the formation of North Atlantic Deep Water (NADW) (Figure **F2**). This single gateway configuration

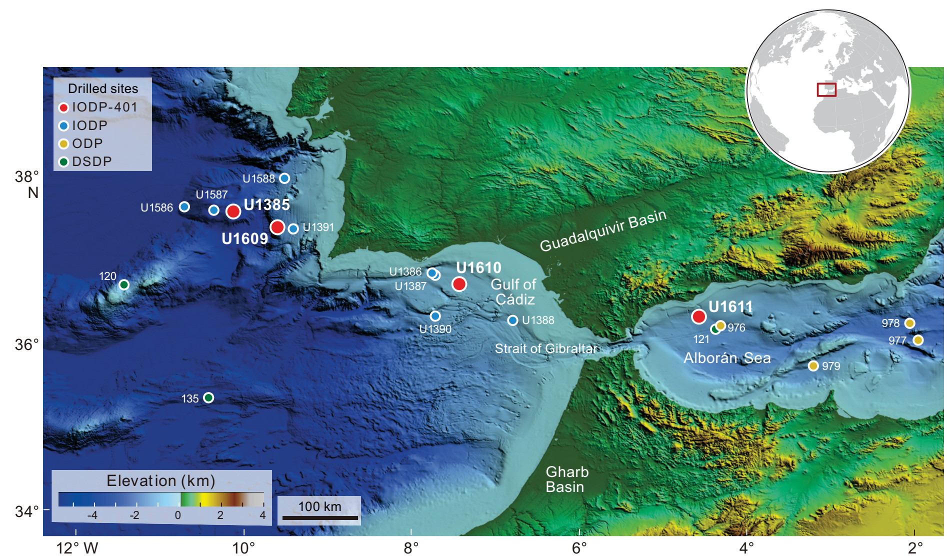

Figure F1. Topographic and bathymetric map of Gibraltar Strait showing locations of Expedition 401 sites and sites from previous expeditions in Atlantic and Alborán Sea. Guadalquivir Basin in Spain and Gharb Basin in Morocco are located at western end of Betic and Rifian Corridors; fossil gateways that closed in Late Miocene and are target of ICDP drilling as part of the IMMAGE Land-2-Sea drilling project. ODP = Ocean Drilling Program, DSDP = Deep Sea Drilling Project.

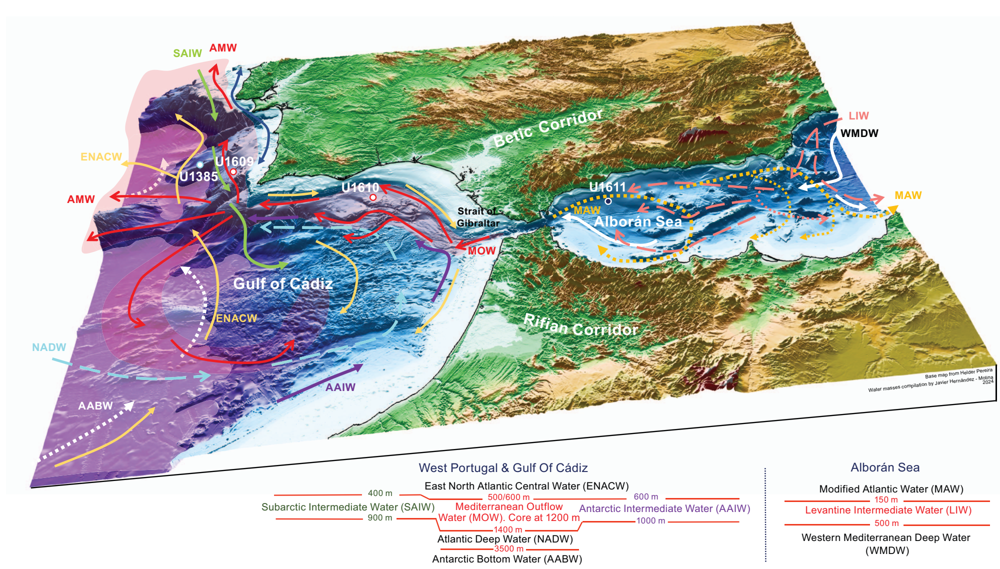

Figure F2. Present-day water mass circulation patterns on either side of Gibraltar Strait in relation to main topographic features and Expedition 401 sites.

only developed in the Early Pliocene. During the Miocene, a wide, open seaway linking the Mediterranean and Atlantic evolved into two narrow corridors: one in northern Morocco and the other in southern Spain (Figure **F3**). Formation and restriction of these corridors permitted Mediterranean salinity to rise and a new, distinct, dense water mass to form and overspill into the Atlantic for the first time. Further restriction and closure of these connections resulted in extreme salinity fluctuations in the Mediterranean, leading to the formation of the Messinian Salinity Crisis (MSC) salt giant. Investigating Miocene Mediterranean–Atlantic Gateway Exchange (IMMAGE) is a Land-2-Sea drilling proposal designed to recover a complete record of Atlantic–Mediterranean exchange from its Late Miocene inception to its current configuration. This will be achieved by targeting Miocene offshore sediments on either side of the Gibraltar Strait during International Ocean Discovery Program (IODP) Expedition 401 and recovering Miocene cores from the two precursor connections now exposed on land during future International Continental Scientific Drilling Program (ICDP) campaigns (Figure **F4**). The scientific aims of IMMAGE are to constrain quantitatively the consequences for ocean circulation and global climate of the inception of Atlantic–Mediterranean exchange, explore the mechanisms for high-amplitude environmental change in marginal marine systems, and test physical oceanographic hypotheses for extreme high-density overflow dynamics that do not exist in the world today on this scale.

2. Background

Paleoclimate research is often driven by the need to validate various types of climate models under boundary conditions different from those of the last 150 y for which an instrumental record of climate is available (Intergovernmental Panel on Climate Change, 2014). Quantifying past changes in temperature, momentum, and flux in the ocean and atmosphere is therefore a key target for geologic research. However, the small size of climate change signals relative to climate proxy measurement uncertainty means this is challenging to achieve (Rohling, 2007). A high signal-to-noise

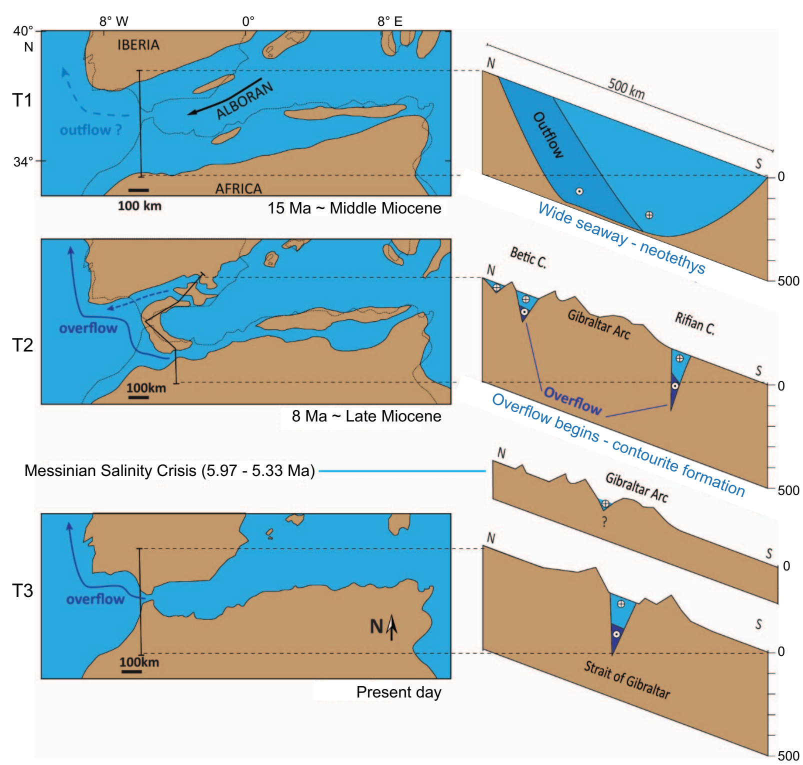

Figure F3. Tectonically controlled reconfiguration of Mediterranean–Atlantic seaways from Middle Miocene to present day. Paleogeography of western Mediterranean after Do Couto et al. (2016). Rifian/Betic seaways (T2), which replaced a wider seaway (T1), are now exposed on land in northern Morocco and southern Spain. T2 scenario (~8 Ma) is the first with potential impact on Atlantic–Mediterranean salinity gradients and overflow formation. (Figure from Capella et al., 2019.)

ratio typically requires amplification of the climate variable, and in the ocean, this is most commonly found in marginal marine basins where exchange with the open ocean is limited so it cannot buffer and diminish the signal of environmental change (Grant et al., 2017). Unfortunately, limited exchange also makes it difficult to use the enhanced marginal basin record to extrapolate to global-scale oceanographic change (Kaminski et al., 2002). Marine gateways linking the basin to the open ocean represent a sweet spot where on one side climatic changes are amplified in the adjoining marginal basin and on the other side their impact on globally meaningful changes in the open ocean can be directly assessed. In addition, the geometric and hydraulic restriction of the gateway itself places physical limitations on the freedom of the system to change (Nelson et al., 1999). This focuses the deposition of the sedimentologic archive of exchange into a small, well-defined geographical area, making it possible to quantitatively constrain responses to exchange that impact global climate (Rogerson et al., 2012b).

The influence of exchanging heat, salt, and momentum through narrow, shallow straits that link the open ocean to marginal basins is profound. The advection of cool or saline waters (Legg et al., 2009) helps drive global thermohaline circulation (Thomas et al., 2004; Álvarez et al., 2005; Rahmstorf, 2006). Because the ocean is the largest of the rapidly exchanging CO_2 reservoirs, this advection also increases the sensitivity of the ocean to atmospheric carbon changes (LaRiviere et al., 2012; Karas et al., 2017; Elsworth et al., 2017; Capella et al., 2019). Although exchange through the Denmark Strait, Indonesian archipelago, and Gibraltar Strait can all overprint both zonal and meridional circulation patterns, global ocean surface circulation and associated heat transport compensating for water mass transformation on the basinward side of gateways forces substantial impacts on sea ice and warming or cooling of adjacent continents and the position of the atmospheric front (Ivanovic et al., 2014a). Unsurprisingly, the opening and closure of oceanic gateways is well recognized as having a profound impact on the Earth's climate, including its periodic switching from greenhouse to icehouse conditions (Kennett, 1982; Smith and Pickering, 2003; Knutz, 2008; Bahr et al., 2022).

The impact of regional changes on global-scale processes are generally ideal questions for Earth System Models experiments. However, because of the inherent small scale of marine gateways relative to global circulation model grid cells, the gateways are either hugely enlarged in the model or the transport of heat and water through them is parameterized rather than explicitly modeled

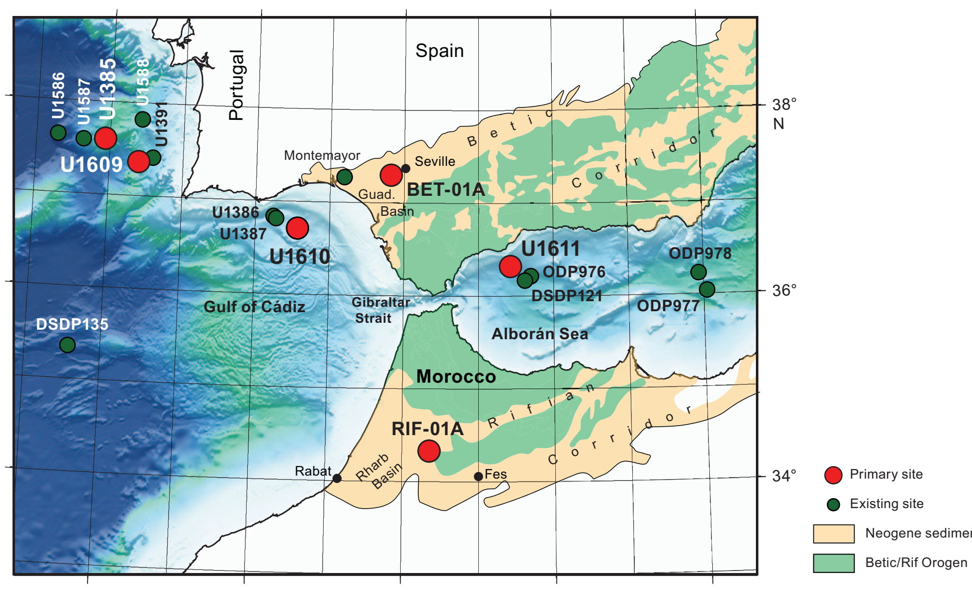

Figure F4. Map of Mediterranean–Atlantic gateway at Gibraltar and two Miocene connections, Betic and Rifian Corridors, that are now exposed on land in Spain and Morocco, respectively. Red circles = IMMAGE Expedition 401 and ICDP drilling targets, green dots = existing IODP/Ocean Drilling Program (ODP)/Deep Sea Drilling Project (DSDP) sites and Montemayor borehole, which recovered Upper Miocene sediments, and closest sites (U1385, U1588, and U1391) that did not reach Miocene.

(e.g., Dietrich et al., 2008; Ivanovic et al., 2013). An excellent example of the problem occurs at Gibraltar (Figure **F4**), where model grid cells of ~400 km^2, which are suitable for the long global simulations necessary for paleoclimate studies, are ill-equipped to simulate hydraulic control in a strait ~15 km in width and consequently generate exchange behavior that differs from observations (Ivanovic et al., 2013; Alhammoud et al., 2010). Consequently, the codependence between ocean and marginal seas in simulations is reduced, preconditioning models to be insensitive to exchange driven change. A view of past and future climate derived from global circulation assessments alone therefore systematically underestimates the role of gateway processes, eliminating a crucial feedback within the Earth system. In summary, exchange through marine gateways is an example of a key climate process that can only be constrained through interrogation of the record of ocean–marginal basin exchange in a specific sedimentary archive.

3. Geologic setting

3.1. Atlantic–Mediterranean exchange now and in the past

In the Atlantic, several marine overflows (Denmark Strait, Mediterranean, and Weddell Sea) supply dense water that collectively feeds the thermohaline circulation system (Smethie et al., 2000; Bahr et al., 2022). The transportation of dense water from the Mediterranean into the interior of the Atlantic (Figure **F2**) is among the largest in the global ocean (Legg et al., 2009), and exchange also provides a key exit point for Atlantic buoyancy, the underlying driver behind Atlantic deep convection (Broecker, 1991).

The dense Mediterranean overflow (MO) is generated as a consequence of its midlatitude setting where evaporation exceeds precipitation (Peixoto and Kettani, 1973), generating a warm, salty water mass. The negative hydrologic budget varies in severity through time, amplifying the climate signal transmitted principally through the Mediterranean's southern catchments and derived from North African monsoon rainfall (Marzocchi et al., 2015). This subtropical monsoonal climate signal with its strong precessional pulse is then propagated into the Atlantic by density driven exchange (Bahr et al., 2015) through the Gibraltar Strait. Water flowing out of the Mediterranean at depth entrains ambient Atlantic water as it goes (Dietrich et al., 2008), generating first Mediterranean Overflow Water (MOW) in the Gulf of Cádiz (Figure **F2**) and Atlantic–Mediterranean Water (AMW) in the rest of the Atlantic (Rogerson et al., 2012b), as well as large depositional and erosional features including extensive sandy contouritic drifts (Figure **F2**) (Nelson et al., 1999; Expedition 339 Scientists, 2013; Hernández-Molina et al., 2003, 2014a, 2014b). AMW flows north, fueling the Norwegian Sea with higher density water that helps sustain the formation and southward flow of NADW (Khélifi et al., 2009; Rogerson et al., 2012b; Kaboth-Bahr et al., 2018).

Despite the challenges of modeling the gateway, the exchange that occurs through the Gibraltar Strait today is a sufficiently influential component of the Earth system for general circulation models to capture at least part of its impact (Bigg et al., 2003; Bigg and Wadley, 2001). Experiments without Atlantic–Mediterranean exchange show that its presence makes Greenland warmer and Antarctica cooler (Bigg et al., 2003). This in turn is sufficient to shift the position of the Intertropical Convergence Zone and, hence, the location of monsoons, storm tracks, and the hyper-arid zones between them. Atlantic–Mediterranean exchange is also a critical component of Atlantic Meridional Overturning Circulation, particularly at times of weak NADW formation (Bigg and Wadley, 2001; Ivanovic et al., 2014a, 2014b; Penaud et al., 2011; Rogerson et al., 2006, 2010; Voelker et al., 2006). Furthermore, the transport of dense water from the Mediterranean into the interior of the Atlantic entrains ambient Atlantic water en route, contributing significantly to global carbon drawdown (2%–5% of today's total net ocean carbon sink; Tans et al., 1993; Siegenthaler and Sarmiento, 1993; Dixon et al., 1994). Taken altogether, this makes Atlantic–Mediterranean exchange a key teleconnection that links African monsoon precipitation derived from the south Atlantic with the northern high latitudes.

Exchange through a single gateway at Gibraltar is a relatively recent phenomenon (Hernández-Molina et al., 2014b; van der Schee et al., 2016; García-Gallardo et al., 2017a, 2017b). As a result of Africa-Eurasia convergence, westward docking of the Alborán plate, and simultaneous slab retreat

(Jolivet and Faccenna, 2000; Faccenna et al., 2004; van Hinsbergen et al., 2014), the Atlantic–Mediterranean connection evolved from a single, wide open seaway (Figure **F3**) linking a Mediterranean that was more of an embayment of the Atlantic than a distinct marginal marine system (Flecker et al., 2015) to two narrow corridors: one in northern Morocco and the other in southern Spain (Benson et al., 1991). The onset of episodic organic-rich sedimentation (sapropels) in the Middle Miocene is the earliest evidence of the Mediterranean operating separately from the Atlantic (Hilgen et al., 2005; Taylforth et al., 2014). Ongoing progressive restriction of the marine corridors permitted Mediterranean salinity to rise, and a distinct, dense water mass formed. This dense water mass overspilled into the Atlantic for the first time at some point during the Middle–Late Miocene (Capella et al., 2017, 2019; de Weger et al., 2020, 2021). Ultimately, the narrowing and closure of these connections resulted in extreme salinity fluctuations in the Mediterranean, leading to the precipitation of more than 1 million km^3 of salt, equivalent to ~6% of the total dissolved oceanic NaCl in the latest Miocene (Blanc, 2006; Ryan, Hsü, et al., 1973). This event is known as the MSC (Hsü et al., 1973). Ongoing tectonic convergence coupled with isostatic rebound related to lithospheric mantle dynamics (Duggen et al., 2003) not only severed these earlier marine connections but also uplifted and exposed them on land (Capella et al., 2017; de Weger et al., 2021). In the Early Pliocene, two-way exchange was established through a single conduit, the Gibraltar Strait (Figure **F3**).

During the MSC, the amplified net evaporative flux changed to such an extent that the salinity of Mediterranean water varied between near-equality with Atlantic water (~36 g/kg) to halite-depositing brine (>360 g/kg) and brackish water conditions (<20 g/kg). Gibraltar exchange today exhibits one of the largest density contrasts in the modern ocean, but this Late Miocene contrast was up to two orders of magnitude higher during the acme of the MSC. The water flowing into the Atlantic at this time was probably the most extremely dense overflow of oceanographic scale in Earth's history, and all other aspects of the exchange would have been proportionally exaggerated.

4. Scientific objectives

The target of the IMMAGE Land-2-Sea drilling project is the record of Atlantic–Mediterranean exchange during the most dynamic and variable period of its history, from inception (~8 Ma) through salt giant formation (6–5 Ma) to the establishment of an exchange configuration similar to today (5–4 Ma). The sediments on either side of the gateway region, which are preserved both on shore and off shore, record the changing nature of Atlantic–Mediterranean exchange, allowing quantitative evaluation of its role in global-scale climate systems, impact on major climatic events, and influence over extreme environmental change in the Mediterranean. Two of IMMAGE's scientific objectives are therefore paleoclimatic. In addition, a Late Miocene drilling target focused on the gateway also provides an unparalleled opportunity to test physical oceanographic representations of extreme high-density overflow dynamics that do not exist in the world today on this scale. IMMAGE's third objective is therefore testing a physical oceanography hypothesis.

4.1. Objective 1: to document the time at which the Atlantic first started to receive a distinct overflow from the Mediterranean and to evaluate quantitatively its role in Late Miocene global climate and regional environmental change

Today, dense water (13°C, 37 g/kg; Price et al., 1993) pools on the floor of the Mediterranean behind a shallow (300 m), narrow (15 km) sill, the Gibraltar Strait (Figure **F4**). Mediterranean waters overspill the sill and cascade down the continental slope (Figure **F2**). The density contrast between Mediterranean and ambient Atlantic water generates substantial current speed, leading to extensive contouritic drifts (Hernández-Molina et al., 2016).

Recent fieldwork in Morocco has revealed that the Rifian Corridor in northern Morocco contains Upper Miocene contouritic sediments (Capella et al., 2017) that resemble the Pliocene–Pleistocene contourites in the Gulf of Cádiz (Expedition 339 Scientists, 2013). The presence of 7.8–6.3 Ma contourites in Morocco (Capella et al., 2017) indicates that an overspill geometry had already formed in the Late Miocene, ~2 My before the MSC, allowing a density contrast between the Mediterranean and Atlantic to develop and feeding saline Mediterranean water into the North Atlantic (Capella et al., 2017, 2019). The outstanding question is whether these exposed Rifian contourites are the first products of MO or whether older, buried contourites exist in either the Rifian and/or Betic Corridors (Figures **F2**, **F3**).

One possibility is that initiation of MO contributed to the cooling that ultimately triggered the formation of permanent Northern Hemisphere ice by altering the North Atlantic density structure and increasing CO_2 drawdown through the entrainment of Atlantic surface water and its dissolved CO_2 in the dense AMW plume (Capella et al., 2019). Correlation with similarly high-resolution sites in the North Atlantic will be required to test this mechanism and assess its importance in modulating NADW formation.

Hypotheses that will be tested as part of this scientific objective include the following:

- Hypothesis 1.1: the earliest contourites formed as a result of Atlantic–Mediterranean exchange and correlate with the onset of Late Miocene sea-surface temperature (SST) decline in the mid- and high latitudes. Dating the first Atlantic–Mediterranean contourites will test this hypothesis.
- Hypothesis 1.2: atmospheric CO_2 sequestration in the deeper ocean through the initiation and development of AMW can account for the degree and distribution of SST cooling observed. Reconstructing the velocity, density, and flux of AMW through time, quantifying its impact on CO_2 advection (Capella et al., 2019), and then modeling the resulting SST distribution (e.g., Ivanovic et al., 2014a) tests this hypothesis.
- Hypothesis 1.3: AMW modulates NADW formation, triggers glacial inception, and influences continental-scale aridification. Model-based testing of this hypothesis requires the correlation of IMMAGE records with existing high-resolution records globally.

4.2. Objective 2: to recover a complete record of Atlantic–Mediterranean exchange before, during, and after the Messinian Salinity Crisis and to evaluate the causes and consequences of this extreme oceanographic event locally, regionally and globally

Today, Mediterranean seawater flows through the Gibraltar Strait forming a saline plume at intermediate depths in the Atlantic (Figure **F2**) (Iorga and Lozier, 1999). The plume's record of Pliocene–Quaternary contouritic sediments was recovered from the Gulf of Cádiz (Integrated Ocean Drilling Program Expedition 339) and documents a Mediterranean contribution to Atlantic thermohaline circulation since the Pliocene (Hernández-Molina et al., 2014b; van der Schee et al., 2016; García-Gallardo et al., 2017a, 2017b). However, there was also a Late Miocene episode of Mediterranean influence on the Atlantic (Capella et al., 2017, 2019), although the conduit for Atlantic–Mediterranean exchange is unclear because Gibraltar may have already been open alongside marine corridors in northern Morocco and southern Spain (Figure **F3**) (Flecker et al., 2015; Martín et al., 2009; Krijgsman et al., 2018) and the Alborán Basin may have been an intermediate system separated from the Mediterranean by the Alborán volcanic arc (Booth-Rea et al., 2018). The sedimentary expression of restriction and closure of these Miocene connections in the Mediterranean comprises both thick evaporite-bearing sequences (e.g., Roveri et al., 2014) and brackish Lago Mare sediments (Iaccarino and Bossio, 1999; Orszag-Sperber, 2006; Rouchy et al., 2007; Guerra-Merchán et al., 2010). Understanding the causes of high-amplitude salinity change in the Mediterranean and its global consequences depends on recovering a complete record of Atlantic–Mediterranean exchange before, during, and after the MSC. Hypotheses that will be tested as part of this scientific objective include the following:

- Hypothesis 2.1: the Alborán Basin was an intermediate marine system influenced by the Atlantic and separated from the Mediterranean by the Alborán volcanic arc during the MSC.
- Hypothesis 2.2: extreme environmental fluctuations in the Mediterranean had negligible impact on AMW.

4.3. Objective 3: to test our quantitative understanding of the behavior of ocean overflow plumes during the most extreme exchange in Earth's history

There are ~20 major ocean-scale overflow systems in the world today (Legg et al., 2009), including some of the most important and sensitive oceanic transport systems (e.g., Denmark Strait and Weddell Sea). All of these systems are driven by source water density anomalies upstream of the overflow (Price and O'Neill Baringer, 1994). However, the range of source water density today is rather small: 27.7 (Red Sea) to 28.95 σ units (Mediterranean Sea). In comparison, the density of Mediterranean water during gypsum and halite deposition would have been enormous (110 and ~300 σ units, respectively). This presents an opportunity and a challenge for existing representations of oceanographic overflow physics (e.g., Legg et al., 2009) because we can test hypotheses derived from physical theory through scientific drilling. The application of physical theory to the paleoceanography of MO is well established (Rogerson et al., 2012a) and suggests the following hypotheses:

- Hypothesis 3.1: the velocity of the plume is a function of the Atlantic–Mediterranean density contrast, limitation on flow through the strait (Bryden et al., 1994), the gradient of the slope, and the degree of mixing (Price et al., 1993).
- Hypothesis 3.2: mixing with ambient water causes a strong negative feedback on the size of the plume, limiting the degree of its variability (Price et al., 1993). This means that only minor changes in the physical size of the plume are expected, despite the proportion of plume water derived directly from the outflow varying significantly. As a result, changes in Mediterranean density have little impact on the plume position.
- Hypothesis 3.3: the main control on the settling depth of MO is the vertical density gradient in the North Atlantic, which is a product of North Atlantic overturning circulation (Rogerson et al., 2012a).

5. Connections to the 2050 Science Framework

Using the newly obtained Expedition 401 cores and those that will be generated by ICDP drilling on land, we will be able to describe the changes in Mediterranean–Atlantic water exchange through geologic time and understand the mechanisms governing those changes and their downstream effects on the Earth's climate system. This will allow us to address the following strategic objectives and initiatives from the 2050 Framework for scientific ocean drilling:

5.1. Strategic objectives

- Earth's climate system: opening and closure of oceanic gateways is recognized as having a profound impact on Earth's climate, changing the distribution of heat and salt in the world's oceans. Dense salty water from the Mediterranean contributes to global thermohaline circulation, NADW formation, and associated carbon drawdown.
- Tipping points in Earth's history: flooding of the Mediterranean basin at the end of the Miocene is one of the most vivid examples of a tipping point in Earth's history. However, the history of water flow through this gateway remains to be described in detail, and it has consequences not just for the Mediterranean but also for the global ocean.
- Global cycles of energy and matter: the Mediterranean–Atlantic gateway has a controlling influence on the distribution of salt, heat, and nutrients in the ocean.

5.2. Flagship initiatives

- Groundtruthing future climate change: sediment cores from this expedition covered the last ~8 My of Earth's climate, including analogs for future warm climates under CO_2 levels up to ~500 ppm. In particular, the combination of gateway and climate history recorded in the cores will help us understand global climate from 8 to 5 Ma, a relatively understudied interval compared to the most recent 5 My.

5.3. Enabling elements

- Broader impacts and outreach: during Expedition 401, we reached a broad audience, communicating the science and real-time progress. Because of the unusually long duration of this Land-2-Sea drilling project, we have an opportunity to develop outreach further.
- Land-2-Sea: this IODP expedition is the first drilling phase of the first Land-2-Sea drilling project to have emerged from an integrated ICDP-IODP proposal evaluation process. The onshore ICDP drilling will happen in the years following Expedition 401 at sites in southern Spain and northern Morocco. Integrated results from both the land and sea drilling are necessary to fully understand Late Miocene gateway history and deliver IMMAGE's scientific objectives. Expedition 401 scientific results provide the foundation on which the two ICDP projects will build.

6. Site summaries

During Expedition 401, core was recovered from seven holes at four different sites (Figures **F5**, **F6**). At Sites U1385 and U1609, where two holes were cored at each site and the physical properties data showed regular cyclic patterns, splices have been constructed.

6.1. Site U1609

6.1.1. Background and objectives

Site U1609 (37°22.6159′N, 9°35.9119′W; proposed site ALM-03B) is located at 1659.5 meters below sea level (mbsl) on the continental slope of the Portuguese margin (Figures **F7**, **F8**; Table **T1**) (see **Background and objectives** in the Site U1609 chapter [Flecker et al., 2025b]). The primary scientific objective of Site U1609 was to recover a distal record of the Late Miocene–Pliocene MO plume (Figure **F2**). The aim was to capture the evolution of the plume's equilibrium depth at this distal location through time, from the earliest evidence of overflow through the Rifian Corridor in present-day Morocco, through the Mediterranean's MSC (5.97–5.33 Ma), to the Early Pliocene

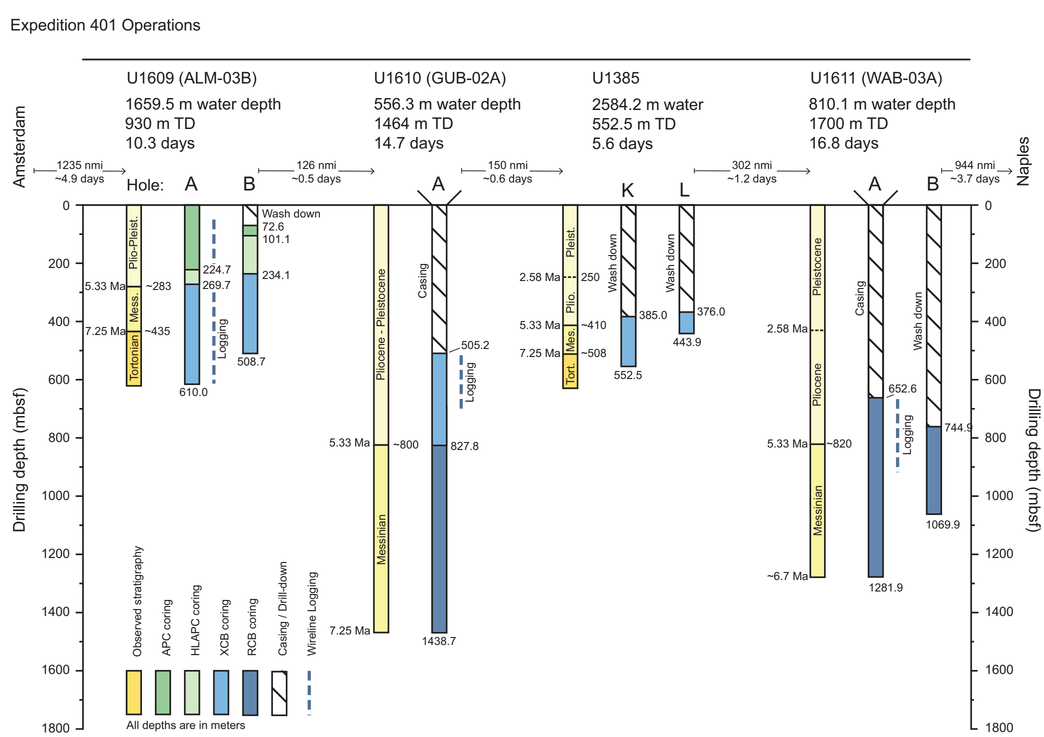

Figure F5. Drilling summary, Expedition 401. Original strategy for these deep holes was to wash down through Pliocene, which had been extensively recovered previously, and core from just above 4.5 Ma bioevent to target depth of 8 Ma. Logging at each site was planned but proved difficult or impossible to implement fully. However, recovery was excellent and there was time to drill a second hole at three of the four sites. TD = total depth.

(~4 Ma). This interval of major gateway and Mediterranean environmental change is likely to have substantially influenced both the density and the chemistry of the overflow on subprecessional to million-year timescales.

Site U1609 is 17 km west and downslope from Integrated Ocean Drilling Program Site U1391 (see Figure **F3** in the Site U1609 chapter [Flecker et al., 2025b]), drilled during Expedition 339, which

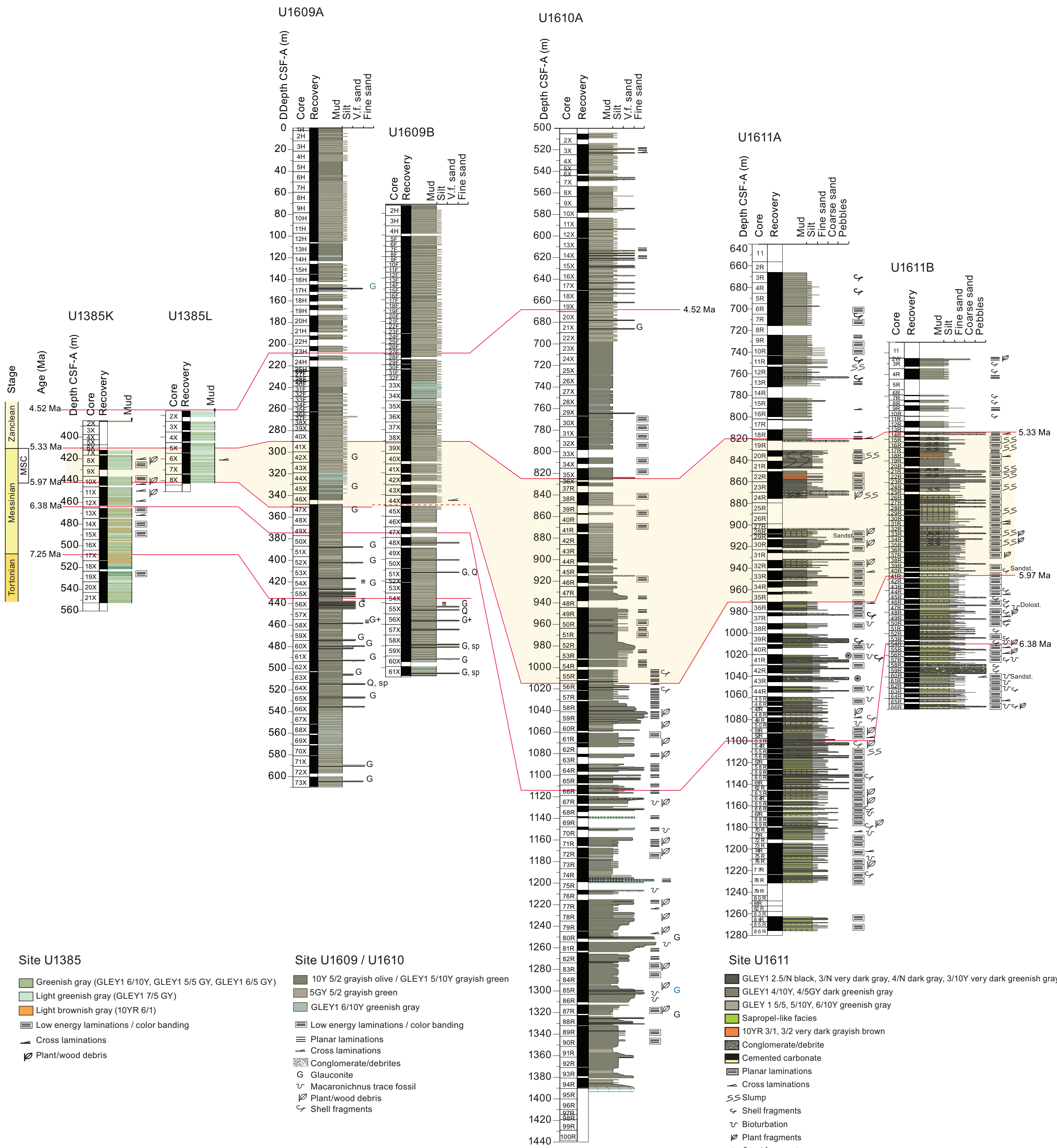

Figure F6. Correlation of lithostratigraphic logs across Expedition 401 sites. Red lines = depth position of key ages horizons at each site, including top and bottom of MSC.

comprises Pliocene–Quaternary muddy contourites with interbedded sands, hemipelagites, and several layers of mass movement deposits. On the seismic profile linking Site U1391 with Site U1609, packages of the contouritic drift migrate landward with time. Site U1609 took advantage of this landward migration and surface erosion to access the target Miocene–Pliocene strata at relatively shallow depths.

Site U1609's distal location was selected to recover a dominantly hemipelagic succession suitable for high-resolution astrochronological tuning providing a strong age framework for subprecessional investigation of the driving mechanisms causing changes in the plume. This record of the Miocene MO plume also provides an important constraint on the upper part of the northeast Atlantic water mass structure in the Late Miocene (Figure **F2**). Data from Site U1609 will be correlated with a deeper water site to the north, Site U1385 (drilled during Expedition 401), and the Miocene successions recovered along the IODP Expedition 397 depth transect (Figure **F4**).

In combination with other Expedition 401 Atlantic sites, the record from Site U1609 also allows the investigation of more specific objectives, including the following:

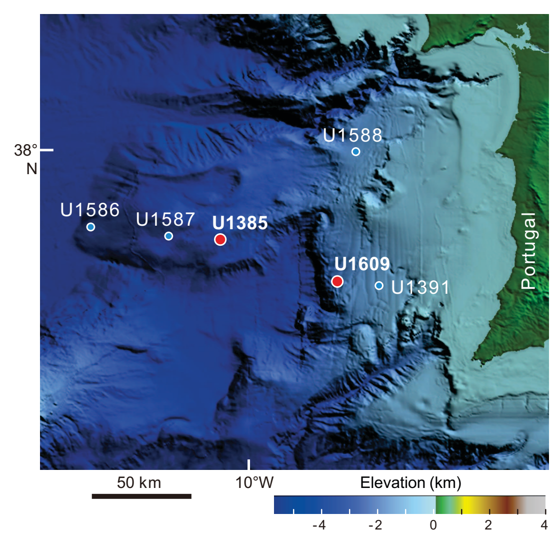

Figure F7. Bathymetric map of Portuguese continental margin showing Sites U1609 and U1385 in relation to previously drilled sites in the area. See Figure F1 for legend.

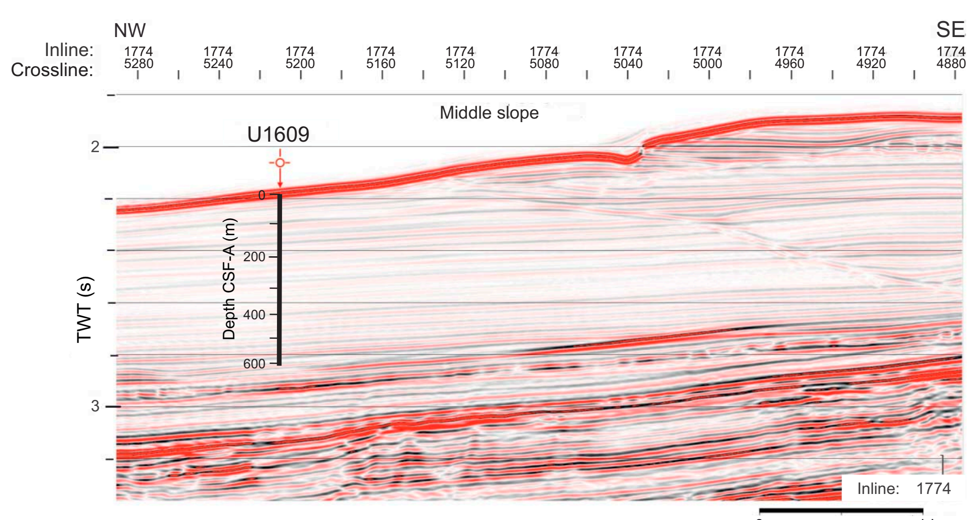

Figure F8. Seismic Profile IL1774 with location and approximate penetration, Hole U1609A.

- To establish the age of the earliest contourites formed as a result of MO,
- To evaluate the impact of extreme environmental fluctuations in the Mediterranean on its overflow plume and the structure of the Atlantic water masses (Figure **F2**), and
- To provide quantitative constraints on the mixing behavior of dense overflows by reconstructing the strength and attenuation rate of the Atlantic–Mediterranean exchange signal beyond the gateway.

6.1.2. Operations

Site U1609 consists of two holes, and 983.0 m of sediment was collected over a 1046.1 m cored interval (Figures **F5**, **F6**). Hole U1609A penetrated 610.0 m with a sedimentary recovered length of 572.2 m (94% recovery). Hole U1609B cored 436.1 m with a sedimentary recovered length of 410.8 m (94%).

6.1.2.1. Hole U1609A

The ship arrived at Site U1609 at 1655 h on 17 December 2023 after completing the 1220 nmi voyage from Amsterdam (Netherlands) in 4.5 days. All thrusters were down and secure at 1712 h, and the ship switched to full automatic dynamic positioning mode at 1720 h, marking the start of operations at Site U1609. Operations started on the rig floor by assembling the bottom-hole assembly (BHA). We used a polycrystalline diamond compact (PDC) drill bit for Hole U1609A, and for the extended core barrel (XCB) cores we used a PDC cutting shoe. This combination was found to yield very good recovery of XCB cores during recent IODP expeditions, including Expedition 397, which drilled in the same area.

At 0430 h on 18 December after one missed mudline, we were successful in starting Hole U1609A (37°22.6259′N, 9°35.9120′W), with the seafloor calculated at 1659.5 mbsl based on the core recov-

Table T1. Hole summary, Expedition 401. — = not applicable. **Download table in CSV format.**

Hole	Latitude	Longitude	Water depth (mbsl)	Total penetration (m)	Drilled interval (m)	Cored interval (m)	Recovered length (m)	Recovery (%)	Total cores (*N*)	APC cores (*N*)	HLAPC cores (*N*)	XCB cores (*N*)	RCB cores (*N*)
U1609A	37°22.6259′N	9°35.9120′W	1659.5	610.0	—	610.0	572.23	94	73	25	12	36	0
U1609B	37°22.6159′N	9°35.9119′W	1659.5	508.7	72.6	436.1	410.75	94	60	3	28	29	0
			Site U1609 totals:	1118.7	72.6	1046.1	982.98	94	133	28	40	65	0
U1610A	36°41.9812′N	7°25.8844′W	556.3	1438.7	505.2	933.5	751.20	80	99	0	0	35	64
			Site U1610 totals:	1438.7	505.2	933.5	751.20	80	99	0	0	35	64
U1385K	37°34.0099′N	10°7.6370′W	2584.2	552.5	385.0	167.5	127.89	76	20	0	0	20	0
U1385L	37°34.0197′N	10°7.6367′W	2584.2	443.9	376.0	67.9	58.44	86	7	0	0	7	0
			Site U1385 totals:	996.4	761.0	235.4	186.33	79	27	0	0	27	0
U1611A	36°18.7537′N	4°34.2717′W	810.1	1281.9	656.3	625.6	431.22	69	85	0	0	0	85
U1611B	36°19.3779′N	4°34.7520′W	784.0	1069.9	744.9	325.0	253.38	78	65	0	0	0	64
			Site U1611 totals:	2351.8	1401.2	950.6	684.60	72	150	0	0	0	149
			Expedition 401 totals:	5905.6	2740.0	3165.6	2605.11	82	409	28	40	127	213

Hole	Latitude	Longitude	Date started	Time started UTC (h)	Date finished	Time finished UTC (h)	Time on hole (h)	Time on site (days)
U1609A	37°22.6259′N	9°35.9120′W	17 Dec 2023	1715	23 Dec 2023	2230	149.25	
U1609B	37°22.6159′N	9°35.9119′W	23 Dec 2023	2230	28 Dec 2023	0000	97.50	
							Site U1609 totals:	10.28
U1610A	36°41.9812′N	7°25.8844′W	28 Dec 2023	1030	12 Jan 2024	0345	353.25	
							Site U1610 totals:	14.72
U1385K	37°34.0099′N	10°7.6370′W	12 Jan 2024	1645	15 Jan 2024	1330	68.75	
U1385L	37°34.0197′N	10°7.6367′W	15 Jan 2024	1330	18 Jan 2024	0730	66.00	
							Site U1385 totals:	5.61
U1611A	36°18.7537′N	4°34.2717′W	19 Jan 2024	1345	30 Jan 2024	1400	264.25	
U1611B	36°19.3779′N	4°34.7520′W	30 Jan 2024	1400	5 Feb 2024	0930	139.50	
							Site U1611 totals:	16.82
							Expedition 401 totals:	47.43

ery and mudline depth in Core 1H. Cores 1H–25H penetrated from the seafloor to 224.7 meters below seafloor (mbsf) and recovered 224.7 m (85%). Advanced piston corer temperature (APCT-3) tool measurements were made during Cores 4H, 7H, 10H, and 13H, and all measurements recorded smooth 10 min long temperature equilibration curves. At 0300 h on 19 December, we switched to the half-length advanced piston corer (HLAPC). Cores 26F–37F penetrated from 224.7 to 269.7 mbsf and recovered 45 m (102%). At 1430 h at 269.7 mbsf, we changed to XCB coring. Cores 38X–73X penetrated from 269.7 to 610.0 mbsf and recovered 340.3 m (99%). Over the course of the hole, the driller pumped eight 30 bbl sepiolite mud sweeps from 274.7 to 571.0 mbsf.

After confirming that early Tortonian sediments had been reached and thus that we had recovered the Messinian to late Tortonian target succession, we stopped coring. The last core, 401-U1609A-73X, reached 610.0 mbsf and came on deck at 2015 h on 22 December.

We prepared the hole for downhole logging by sweeping it with 30 bbl of sepiolite mud to flush out any loose sediment, displacing it with 230 bbl of barite-weighted mud to stabilize the borehole walls, and setting the end of the pipe to 56.4 mbsf. The triple combo downhole logging tool string was assembled by 0130 h on 23 December, but before it could be run down the pipe, the wireline heave compensator control computer was found to be unresponsive. After troubleshooting diagnosed a probable hard drive failure, we decided to log without heave compensation. Ship heave was around 2.5 m throughout the day—higher than desirable but not atypical for logging from the ship. The triple combo logged borehole physical properties data down to within 5 m of the bottom of the hole. The second tool string, the Versatile Seismic Imager, also reached close to the bottom of the hole for the check shot survey. Concurrently, we observed for protected marine species; none were observed. Only 2 of the 13 check shot stations gave reliable first-arrival times because most of the borehole was too wide to achieve good coupling. Fortunately, those two stations were in the lower part of the hole where the data are most useful for tying borehole depth to the seismic profiles. Because of the wide borehole and the lack of heave compensation, we decided not to run the Formation MicroScanner tool and instead to run a sonic velocity and natural gamma radiation (NGR) tool string as the third and final logging run. This tool string also reached close to the base of the hole. The logging equipment was rigged down by 2230 h on 23 December. We raised the pipe, and the bit cleared the seafloor at 2235 h, ending Hole U1609A.

6.1.2.2. Hole U1609B

The ship was offset 20 m south of Hole U1609A along the slope, and at 0305 h on 24 December 2023 we started Hole U1609B (37°22.6159′N, 9°35.9119′W) by drilling down without recovery. The plan was to drill down without coring to spend more time coring the Early Pliocene to Late Miocene target interval; however, in these clay-rich sediments, drilling was no faster than taking cores. At 0930 h, we retrieved the center bit and started taking advanced piston corer (APC) cores at 72.6 mbsf. Cores 2H–4H penetrated from 72.6 to 101.4 mbsf and recovered 28.5 m (95%), but after Core 4H had partial recovery and required 20,000 lb overpull to retrieve, we switched to coring with the HLAPC coring system at 101.1 mbsf. Cores 5F–32F penetrated from 101.4 to 234.1 mbsf and recovered 133.0 m (101%). We ran the Sediment Temperature 2 (SET2) tool after Core 32F at 234.1 mbsf to measure formation temperature deeper than had been possible with the APCT-3 tool in Hole U1609A.

At 1630 h on 25 December, we switched to the XCB coring system. At 1600 h on 26 December after taking Core 401-U1609B-48X at 389.3 mbsf, we ran the SET2 tool a second time. XCB coring proceeded until cores reached the age of 8.4 Ma, old enough to cover the main events in the history of the Mediterranean–Atlantic gateway. Cores 33X–61X penetrated from 234.1 to 508.7 mbsf and recovered 264.9 m (91%). At 1700 h on 27 December, we set back the top drive and started to pull up the drill pipe. The bit cleared the seafloor at 1905 h, and the BHA was on deck by 2345 h. The thrusters were raised, and we started the transit to Site U1610 at 2354 h, ending Site U1609.

Overall, we spent 10.2 days at Site U1609, about 2 days fewer than in the original operations plan because the age targets were shallower than anticipated. For this reason, we were also able to recover two cored records of the target interval rather than the single core record that was originally planned in Flecker et al. (2023).

6.1.3. Principal results

6.1.3.1. Lithostratigraphy

Three main lithologies are described at Site U1609: calcareous mud, calcareous silty mud, and clayey calcareous ooze. Minor coarser grained deposits (e.g., calcareous silt, sandy silt, and calcareous sand) are also observed. On the basis of subtle lithologic changes, Holes U1609A and U1609B are divided into four lithostratigraphic units (Figure **F9**). Contacts between these units and the lithologies within them are mainly gradational, characterized by subtle changes in color and grain size (Figure **F10**). Only the coarser silts and sandier beds are characterized by sharp to erosive basal contacts. In Hole U1609A, Unit I (0–344.0 mbsf) is characterized by alternating calcareous mud and calcareous silty mud. Unit II (344.0–457.7 mbsf) consists of alternating calcareous mud and clayey calcareous ooze. Unit III (457.7–531.5 mbsf) contains cyclic triplets of calcareous mud of two different shades (lighter/darker) and clayey calcareous ooze, repeating on a meter scale. Unit IV (531.5–609.3 mbsf) contains two distinct types of calcareous muds and clayey calcareous

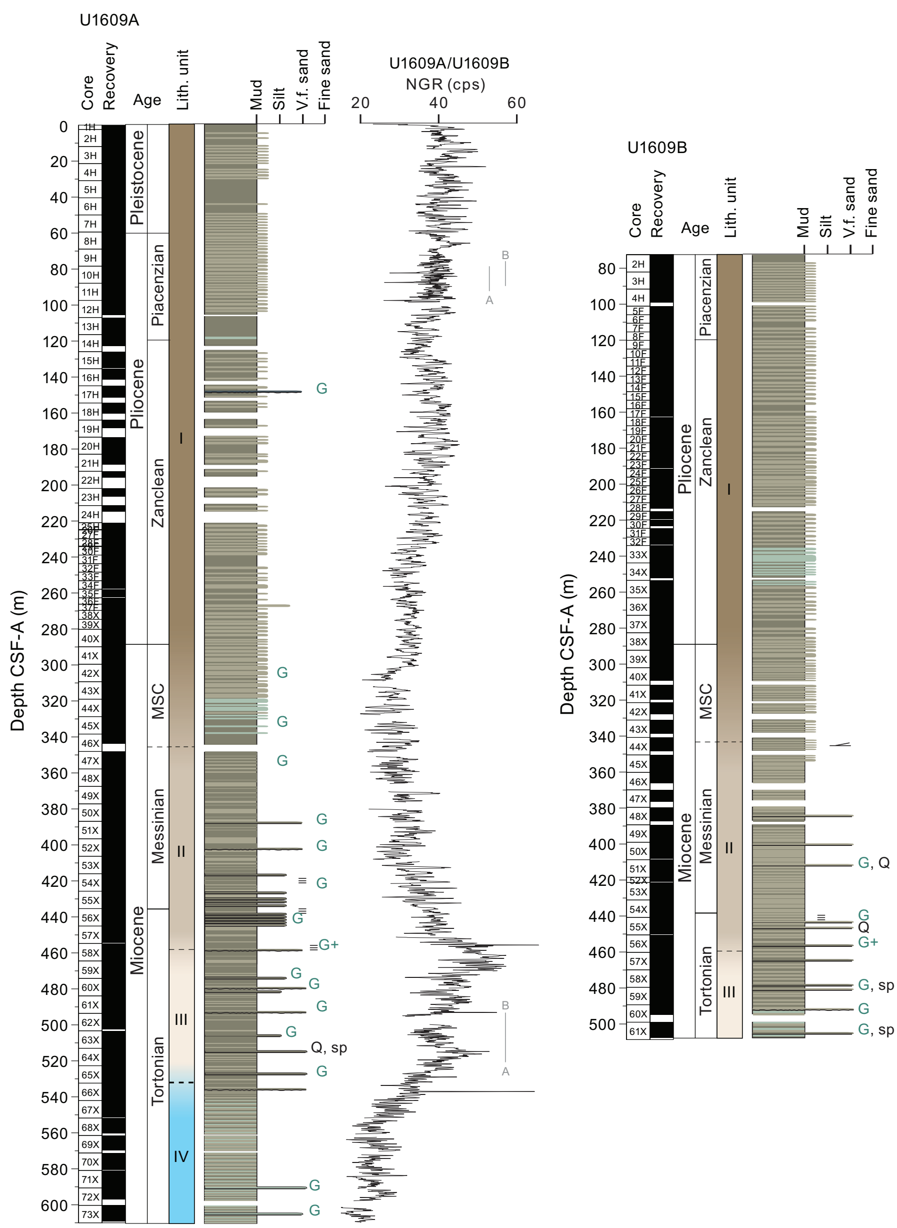

Figure F9. Site U1609 synthesis. NGR data shown is derived mainly from Hole U1609B, with upper and lower intervals from Hole U1609A. See Figure F6 for lithology and symbol legend. V.f. = very fine. Labeled vertical lines = transition between hole NGR data sets. cps = counts per second.

ooze, with brown calcareous muds as the dominant lithology. In this unit, bed thickness is usually <1 m and the beds occur rhythmically. Coarser sandy and silty deposits at ~10 cm scale are observed primarily in Units II and III.

Units I–III were recovered in Hole U1609B (Figure **F9**). The thickness of these units and the sedimentary characteristics observed within them closely resemble those found in Hole U1609A.

The sedimentary facies and facies associations identified at Site U1609 can be mainly attributed to hemipelagic and bottom current processes. This site recovered part of the Sines drift (middle-slope plastered drift) during deposition of Unit I (Pliocene and late Messinian). Beneath this, a few early Messinian and the Tortonian turbidite deposits are intercalated (Units II–IV). These coincide with regional tectonic events (Suárez Alba et al., 1989; Riaza and Martínez Del Olmo, 1996; Sierro et al., 1996; Maldonado et al., 1999; Ledesma, 2000; Martínez del Olmo and Martín, 2016); however, relative sea level falls may also have triggered gravity flows during this time interval.

The regular cyclicity visible in both the sedimentary facies and the physical properties data may be explained by local precessional climatic fluctuations as well as bottom current variability. Bottom currents during deposition of Unit I were weak but vigorous enough at intermediate depths to develop a plastered drift along the middle continental slope. On the longer timescale, trace fossil assemblages indicate Tortonian to Pliocene shallowing. This may be related to long-term sea level regression (landward) and later progradation (basinward) of the margin (Riaza and Martínez Del Olmo, 1996; Sierro et al., 1996; Maldonado et al., 1999; Ledesma, 2000; Martínez del Olmo and Martín, 2016).

6.1.3.2. Biostratigraphy

The sedimentary record recovered at Site U1609 is mostly continuous, although minor discontinuities cannot be totally excluded based on the low resolution of the biostratigraphic sampling on

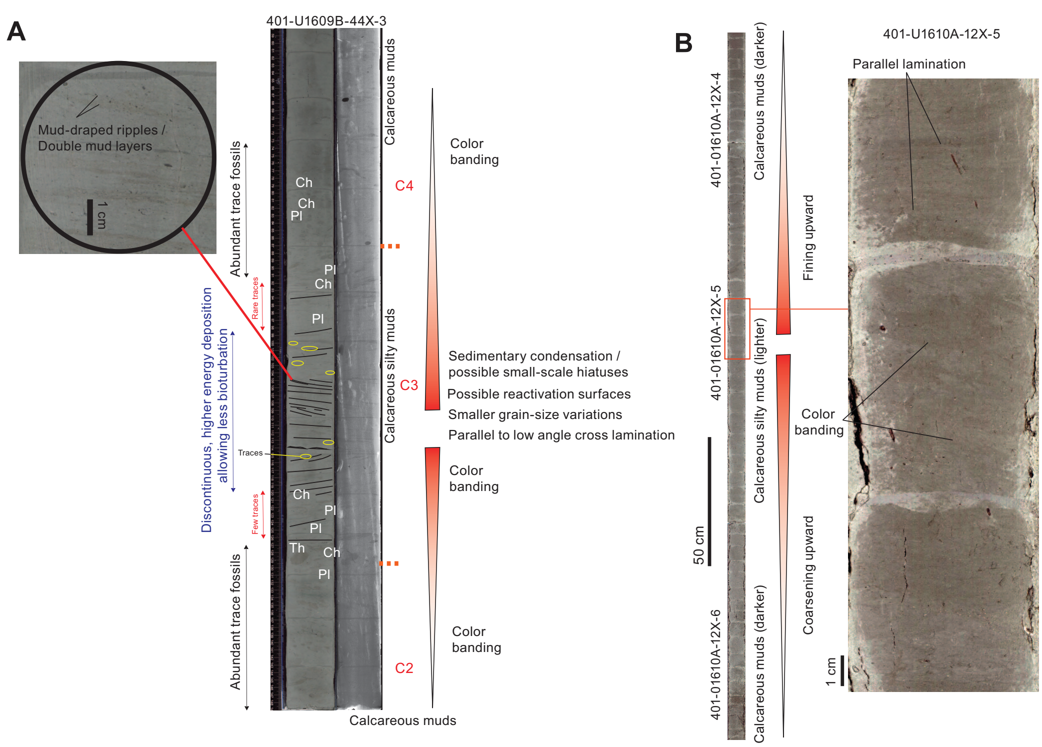

Figure F10. Examples of bigradational sequences of contourites. A. Fine-grained contourite with typical expression of subtle lithologic change observed (left: linescan; right: XSCAN), Site U1609. This section is a rare example showing trace fossil distribution, primary sedimentary structures, and subdivision intervals (C1–C5) according to contourite facies model for bigradational sequences (Stow and Faugères, 2008). Ch = *Chondrites*, Pl = *Planolites*, Th = *Thalassinoides*. Yellow circles = discrete traces on central interval of bigradational sequence. B. Fine-grained contourite showing coarsening- and fining-upward sequence, as well as some subtle sedimentary structures, such as parallel lamination and small grain size variations, Site U1610.

board. Preservation of microfossils is generally good with abundant calcareous nannofossils and planktonic foraminifers; benthonic foraminifers are rare.

Based on the calcareous nannoplankton assemblage, the top of the sequence recovered in Hole U1609A is estimated to be >1.24 Ma, indicating that a significant proportion of the Pleistocene sequence has been eroded at this location. A continuous series of calcareous nannoplankton and planktonic foraminifer events were recorded at this site spanning the early Pleistocene to the earliest Tortonian (Figure **F9**). Some of the calcareous nannofossil bioevents, specifically the highest occurrence (HO) events, may have been affected by reworking and redeposition. However, the ages derived from both the nannofossils and the foraminifers suggest that this is not a major issue. Sedimentation rates combined with the oldest bioevent, suggest an age close to the Tortonian/Serravallian boundary for the base of Hole U1609A.

During the Pliocene, bioevent-derived sedimentation rates range 37–90 m/My, which is in line with those estimated from the paleomagnetic records. Miocene successions have lower sedimentation rates (39–71 m/My).

6.1.3.3. Paleomagnetism

Paleomagnetic investigation of cores from Holes U1609A and U1609B focused on demagnetization of the natural remanent magnetization (NRM) of archive-half core sections and discrete samples of the working-half core sections. The Icefield MI-5 core orientation tool was used to orient the uppermost 24 cores in the APC-cored interval of Hole U1609A. The NRM intensity is very weak, ranging from about 1.4×10^{-5} to 4.0×10^{-1} A/m with an average of 2.5×10^{-3} A/m.

In Hole U1609A, NRM removed by 10 mT alternating field (AF) demagnetization is likely related to an overprint caused by core drilling. Inclination values after 10–20 mT AF demagnetization roughly show polarity reversals but with a lot of values scattered between expected normal and reversed values and with very few of the reversed values reaching the expected geocentric axial dipole (GAD) inclination at the site (56.7°). The weak magnetization and scattered directions may be due to dissolution of most of the original magnetic minerals and precipitation of authigenic iron sulfides. However, after running a 1 m smoothing window on the inclination values, normal and reversed polarity intervals can be tentatively recognized and constrained by the biostratigraphic framework, correlated to the geomagnetic polarity timescale (GPTS) from about 1.2 to 8.7 Ma.

6.1.3.4. Geochemistry

Salinity, pH, alkalinity, concentrations of major anions and cations, ammonium, phosphate, and trace elements were measured on 66 interstitial water (IW) samples and a mudline (bottom water) sample from Hole U1609A. IW was extracted by squeezing a 5–7 cm whole-round sample, and the squeeze cake residues were then sampled for sedimentary geochemistry. One IW sample was collected from every APC and XCB core (401-U1609A-1H through 25H and 38X–73X), and one sample was collected from every other HLAPC core (Cores 28F–36F). Alkalinity increased from 2.4 mM at the mudline to >15 mM between 44.8 and 256.1 mbsf, driven primarily by sulfate reduction, and pH varied between 7.4 and 7.8. Major ion concentrations, nutrient concentrations, and alkalinity reflect a variety of subsurface diagenetic processes, including sulfate reduction, carbonate mineral precipitation and dissolution, organic matter remineralization, and water uptake into clay minerals. The sulfate–methane transition zone occurs around Core 6H at ~45 mbsf.

Weight percent total inorganic carbon (TIC), sedimentary carbon (total carbon [TC]), and total nitrogen (TN) were measured on the squeeze cake residues from the Hole U1609A IW sampling. Headspace gas was also measured from a discrete sample taken at the top of the core section below each of the 66 IW samples. Methane and ethane were commonly detected, whereas ethene and propane were detected in trace amounts in <10 samples. Methane concentrations ranged 0–42,690 parts per million by volume (ppmv), and ethane concentrations ranged 0–3.3 ppmv, with highest abundances between 100 and 300 mbsf. Calcium carbonate content ($CaCO_3$ wt%) was calculated from the TIC content, assuming that all inorganic carbon is present as calcium carbonate. Total organic carbon (TOC) was determined as the difference between TC and TIC. Calcium carbonate varied between 20 and 75 wt%, increasing toward the bottom of Hole U1609A, whereas TOC and TN remained low (<1% and <0.08%, respectively) throughout.

6.1.3.5. Physical properties and downhole measurements

Analysis of physical properties data allowed us to define four units at Site U1609 that correspond to the lithostratigraphic units (Figure **F9**). In general, there is a correlation between magnetic susceptibility (MS), NGR, and gamma ray attenuation (GRA) bulk density, all presenting a slight decrease from the top to the bottom of Unit I. Unit II shows an increasing trend for both NGR and GRA toward the bottom of the unit (458 mbsf). Unit III contains several coarser sandy layers and is followed by greater variations on physical properties that present a global decreasing trend toward the bottom of the unit (531 mbsf). Unit IV represents a decrease in all the measured physical properties. This is reflected in the sedimentologic data by the transition to a less siliciclastic sequence of clayey calcareous oozes and calcareous muds. Generally, variations in physical properties are associated with color changes in the visual core descriptions and in the red-green-blue (RGB) and reflectance data. This suggests that color changes are associated with changes in grain size and mineralogical composition.

Logging data from the downhole logging operations in Hole U1609A were processed at Lamont-Doherty Earth Observatory, Columbia University (USA). The sonic velocity logs and check shot interval velocity values reached 2.25 km/s at the base of the logging interval (578 mbsf). These in situ velocity data enabled the Hole U1609A stratigraphy to be more accurately tied to the seismic stratigraphy. Based on downhole temperature measurements, the seafloor temperature is 6.9°C.

6.2. Site U1610

6.2.1. Background and objectives

Site U1610 (proposed Site GUB-02A) is the closest of the expedition's Atlantic sites to the Gibraltar Strait and by extension to the Mediterranean–Atlantic gateway during the Late Miocene (Figures **F4**). It is located at 556.3 mbsl in the Gulf of Cádiz (36°41.9812′N, 7°25.8844′W; Table **T1**) (see **Background and objectives** in the Site U1610 chapter [Flecker et al., 2025c]). The aim of drilling at Site U1610 was to provide a proximal record for the proximal–distal transect along the path of the MO plume during the Late Miocene and Early Pliocene (Figure **F2**).

There is considerable uncertainty about the Late Miocene timing of opening and closure of the three different Mediterranean–Atlantic gateways (the Betic corridor through southern Spain, the Gibraltar Strait, and the Rifian corridor through Morocco) (Figure **F3**) (Krijgsman et al., 2018), and establishing this history is one of the main objectives of the expedition. Site U1610 was positioned at a location that would capture a record of Mediterranean overflow wherever it was coming from, throughout the 8–4 Ma interval of interest. The Miocene target interval also needed to be sufficiently shallowly buried (<1700 mbsf) and in deep enough water to be accessible to the R/V *JOIDES Resolution* drilling capability. However, the Pliocene–Pleistocene succession in the Gulf of Cádiz derives both from more recent MO and substantial clastic deposition from mainland Spain and Portugal, so in many places this Miocene–Pliocene interval of interest is too deeply buried. Additionally, all potential IODP sites need to be in locations where hydrocarbon accumulations are demonstrably absent, which is particularly challenging in the Gulf of Cádiz. Within these constraints, there was little choice about the location of Site U1610, and even here the target depth of 1460 mbsf was very deep for IODP drilling (Figures **F5**, **F11**).

The two-way traveltime (TWT) to depth conversion used for the Pliocene–Pleistocene succession at Site U1610 was derived from adjacent Expedition 339 Sites U1386 and U1387 (Expedition 339 Scientists, 2013), which lie ~20 km northwest (see Figure **F4** in the Site U1610 chapter [Flecker et al., 2025c]). This indicated that the Pliocene–Pleistocene succession at Site U1610 was ~750 m thick. Our drilling strategy was to drill ahead without coring the Pleistocene and the top of the Pliocene, which were already recovered during Expedition 339, casing the hole to 550 mbsf to increase the chances of recovering the target interval.

Site U1610 is located in the Deep Algarve Basin of the Gulf of Cádiz (Ng et al., 2022). Based on regional correlations to Expedition 339 sites and industry wells, the Late Miocene seismic stratigraphic sequence at the site location charts the progradation of a submarine fan (channel/levee/lobes system) influenced by bottom currents. The seismic packages transition upward from distal submarine lobes to more proximal, coarser grained submarine lobes, which are overlain by a transparent unit thought to reflect hemipelagic deposition and then a Pliocene–Pleistocene MO-derived contouritic drift. At the base of this sequence (around 2.1 s TWT) (see Figure **F6** in the Site U1610 chapter [Flecker et al., 2025c]) is a wedge-shaped, chaotic unit that is interpreted to be the toe of an olistostrome, equivalent to the olistostrome seen in outcrop in southern Spain. The 8 Ma target age was anticipated to lie just below this chaotic interval.

6.2.2. Operations

Site U1610 consists of one hole, U1610A, and 751.2 m of sediment was collected from over a 933.5 m cored interval (81% recovery). The upper 501.9 m of the hole was cased to prevent caving and make it easier to flush cuttings out of the borehole (Figure **F5**), with the aim of increasing the chances of coring and logging successfully to the target depth of 1460 mbsf.

6.2.2.1. Hole U1610A

The ship completed the 122 nmi voyage to Site U1610 at a speed of 11.5 kt, arriving at 1010 h on 28 December 2023. The hydraulic release tool (HRT) and casing were prepared, consisting of the HRT assembly, HRT base, and 498 m of 10¾ inch casing. The rig team then made up the BHA, including the bit, underreamer bit, and mud motor. The BHA and drill pipe were lowered through the casing until the bit and underreamer extended below the casing by 3 m. The HRT running tool was attached to the casing, and the funnel was welded on; after that, the entire casing system was lowered through the moonpool and the ship was positioned over the hole coordinates.

Hole U1610A started at 1200 h when the seafloor was tagged at 561.7 mbsl. The funnel's base landed on the seafloor with the casing shoe at 501.9 mbsf. After the casing was released, the bit was raised, clearing the seafloor at 2215 h on 30 December and clearing the rotary table at 0302 h on 31 December, completing casing operations.

We elected to start coring in Hole U1610A with the XCB coring system because it recovered good quality cores at equivalent depths in Hole U1609A. The nonmagnetic drill collar was left out of the assembly to improve the robustness of the BHA, and a lockable float valve was included for potential downhole logging.

Hole U1610A was reentered at 0940 h on 31 December, and during this process the depth to the seafloor was found to be 556.3 mbsl, identical to the precision depth recorder (PDR) reading but shallower than the previous estimate of 561.7 mbsl. The bit was lowered to the base of the hole (505.2 mbsf), and the first science activity at the site was to run the SET2 tool. At 1430 h, we started coring Core 2X and continued into the new year.

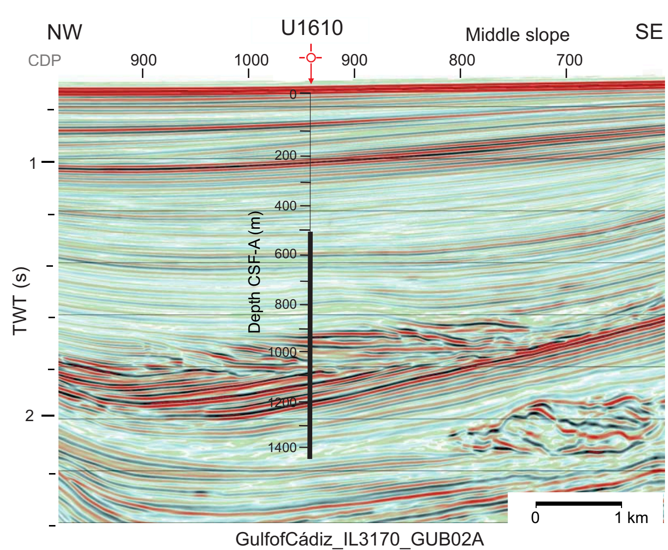

Figure F11. Seismic Profile IL3170 with location and approximate penetration, Hole U1610A. CDP = common depth point.

At 0340 h on 4 January 2024, we started a more rigorous headspace gas sampling protocol for the interval 754–960 mbsf at this site, following a recommendation by the IODP Environmental Protection and Safety Panel and Texas A&M University Safety Panel. Beginning with Core 401-U1610A-27X at 747.7 mbsf, the headspace gas results from each core were analyzed before advancing the bit to collect the next core. This protocol was in effect because a detailed preexpedition analysis of 3D seismic data showed that there is a nonzero but very low risk of finding gas at the Site U1610 location. Headspace gas results from all XCB cores were found to be in the normal (safe) range of methane/ethane ratios and absolute methane values. Cores 2X–36X penetrated from 505.2 to 827.8 mbsf and recovered 322.6 m (93%).

At 0700 h on 4 January, there was a failure in the top drive brake system, causing the brake to engage and overheat. We stopped coring and pulled up Core 3401-U1610A-6X, which had advanced 3 m. The bit was raised to 793.5 mbsf, the top drive was racked to allow repair, and the bit was raised to 495.2 mbsf just inside the casing. The first interval of top drive inspections and repair ran from 0945 to 1330 h. The cause for the failure appeared to be the exhaust valve on the brake. A portion of the diaphragm in the exhaust valve had broken off, lodged in the valve, and kept air pressure to the energizing bladder behind the brake bands. This kept the brake engaged. There was significant damage to the brake and bladder assembly from the resultant overheating, and the entire brake assembly needed to be replaced with the spare unit from the warehouse.

Meanwhile, we decided to change from the XCB system to the rotary core barrel (RCB) system for the remainder of the hole. We raised the bit to the ship, clearing the seafloor at 1423 h and the rig floor at 1630 h on 4 January. Repairs to the top drive continued and were complete by 0215 h on 5 January. The rig floor team then assembled the RCB BHA with a new 9⅞ inch PDC bit, and Hole U1610A was reentered at 0548 h. Core 50R marked the end of the special headspace gas protocol, and results were within the normal range for the interval where the enhanced gas safety protocol was in effect. The procedure resulted in a delay of ~45 min per core across 23 cores.

Coring continued with very good recovery to Core 401-U1610A-95R, which recovered just 15 cm of hard dolostone rock pieces. Core 96R was empty, so we ran the bit deplugger to remove any potential obstructing rock lodged in the bit. Although the drilling rate indicated that we were drilling recoverable sediments and had passed below the hard lithified sediments that had been partly recovered in Core 95R, no sediments were recovered; therefore, we stopped coring at 0515 h on 11 January with Core 100R. Cores 37R–100R penetrated from 827.8 to 1438.7 mbsf and recovered 610.9 m (74%).

We prepared for downhole logging by releasing the bit at the bottom of the hole, filling the hole with 354.3 bbl of heavy (10.5 lb/gal) barite mud, and raising the pipe. When the end of the pipe reached 779.4 mbsf, the drill pipe became stuck. After an overpull of 60,000 lb would not free the pipe, the circulating head was attached so that fluid could be pumped and the top drive was picked up so that the pipe could be rotated. After several attempts, the pipe came free at 1215 h on 11 January with 90,000 lb overpull and a pump pressure of 600 psi. The end of the pipe was set at 516.6 mbsf for logging, 14.7 m below the casing shoe.

At 1415 h on 11 January, we started to assemble the quad combo tool string, including NGR, density, resistivity, and sonic velocity tools. The tool string was lowered down the hole, passing out of the casing into the open hole at 1640 h. At ~726 mbsf, the tool string encountered an obstruction, and after eight attempts, it could not pass any farther down the hole. This is the same depth interval at which the drill pipe was stuck earlier in the day. However, useful log data were acquired from the ~208 m open hole logged interval.

The inclinometer in the cablehead of the quad combo logging tool string showed that Hole U1610A was inclined between 13° and 15° from vertical in the logged interval. The hole had been suspected to deviate from vertical from observations of inclined beds in the cores.

The downhole logging equipment was rigged down by 0045 h on 12 January, and the pipe was raised, clearing the seafloor at 0130 h and the rig floor at 0300 h. The rig floor was secured for transit, we raised the thrusters at 0336 h, and we started the sea passage to Site U1385 at 0348 h, ending Site U1610.

6.2.3. Principal results

6.2.3.1. Lithostratigraphy

Seven primary lithologies were described in Hole U1610A: calcareous clay, calcareous mud, calcareous silty mud, calcareous (sandy) silt(stone), calcareous (silty) sand(stone), clayey calcareous ooze, and dolostone. Minor coarser grained lithologies were also observed. Based on these lithologic descriptions, Site U1610 is divided into five lithostratigraphic units (Figure **F12**). Contacts between lithologies are predominantly gradual, with subtle color and grain size changes; however, some contacts are sharp to erosive.

Unit I (505.2–699.4 m core depth below seafloor, Method A [CSF-A]) is composed of alternating calcareous mud and calcareous silty mud, with minor coarser, sandy intervals. Unit II (699.2–

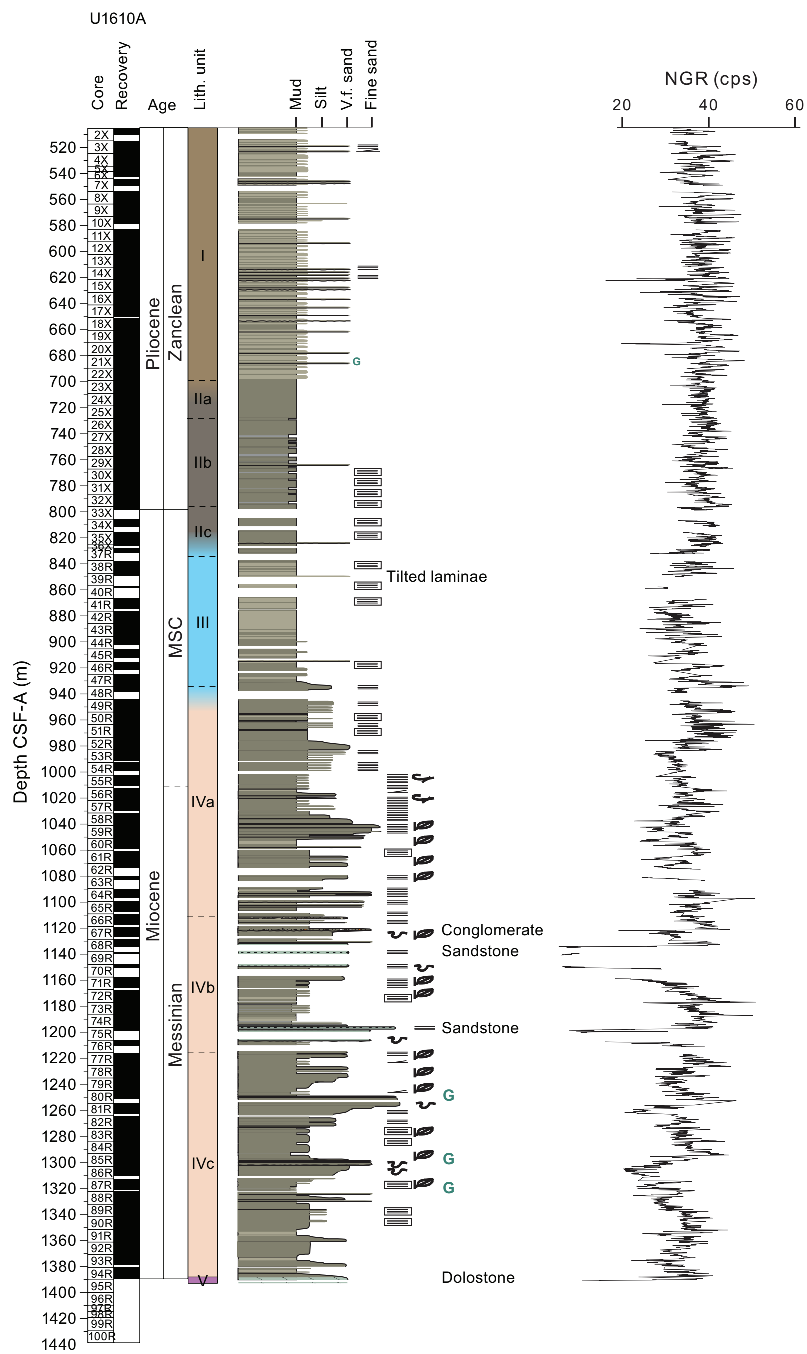

Figure F12. Site U1610 synthesis. See Figure F6 for lithology and symbol legend. V.f. = very fine. cps = counts per second.

835.0 m CSF-A) consists of calcareous mud and calcareous clay that is divided into three subunits. Subunit IIa is composed entirely of calcareous mud (699.4–728.3 m CSF-A), Subunit IIb is composed of alternating calcareous mud and calcareous clay (728.3–796.4 m CSF-A), and Subunit IIc is predominantly composed of calcareous mud (796.4–835.0 m CSF-A). Unit III (835.0–934.5 m CSF-A) consists of interbedded calcareous mud and clayey calcareous ooze to calcareous silty mud, with minor coarser, sandy intervals. Unit IV (934.5–1388.8 m CSF-A) is divided into three subunits (Figure **F12**). Subunit IVa consists of alternating calcareous silty mud, calcareous sandy silt, calcareous mud, and coarser grained sand and silty sand intervals (Figure **F13**), with minor clayey calcareous ooze to calcareous clay (934.5–1112.7 m CSF-A). Subunit IVb consists of calcareous mud, calcareous silty mud, calcareous sandy silt, and calcareous sand (very fine, fine, and medium), with some clayey calcareous ooze to calcareous clay and minor lithified siltstone, sandstone (fine to medium), and conglomerate (1112.7–1220.3 m CSF-A). Subunit IVc consists of alternating calcareous mud, calcareous silty mud, calcareous sandy silty, and coarser grained sand and silty sand intervals, with minor clayey calcareous ooze to calcareous clay and calcareous clay (1220.3–1388.8 m CSF-A). Unit V (1388.8–1390.6 m CSF-A) consists entirely of dolostone. Cores 401-U1610A-96R through 100R (1390.6–1438.7 m CSF-A) recovered no sediments, and this interval is not included in the unit definition.

Hole U1610A is located in the southern part of the Deep Algarve sedimentary basin in the Gulf of Cádiz. During deposition of Unit IV in the early to late Messinian (<6.9–7.1 Ma to around 5.78 Ma), there was an interplay of gravity processes, (contouritic) bottom currents, and pelagic/hemipelagic deposition that resulted in a mixed (turbidite-contourite) depositional system, where turbiditic deposits were reworked by bottom currents. The bottom current processes are associated with an intermediate water mass flowing along the middle slope of the margin. This mixed depositional system underwent a long-term evolution from Subunit IVc to Subunit IVa. These sediments display a wide range of features and deposits formed under synchronous and asynchronous interactions of gravity and contouritic processes. Turbidite deposits have been described in

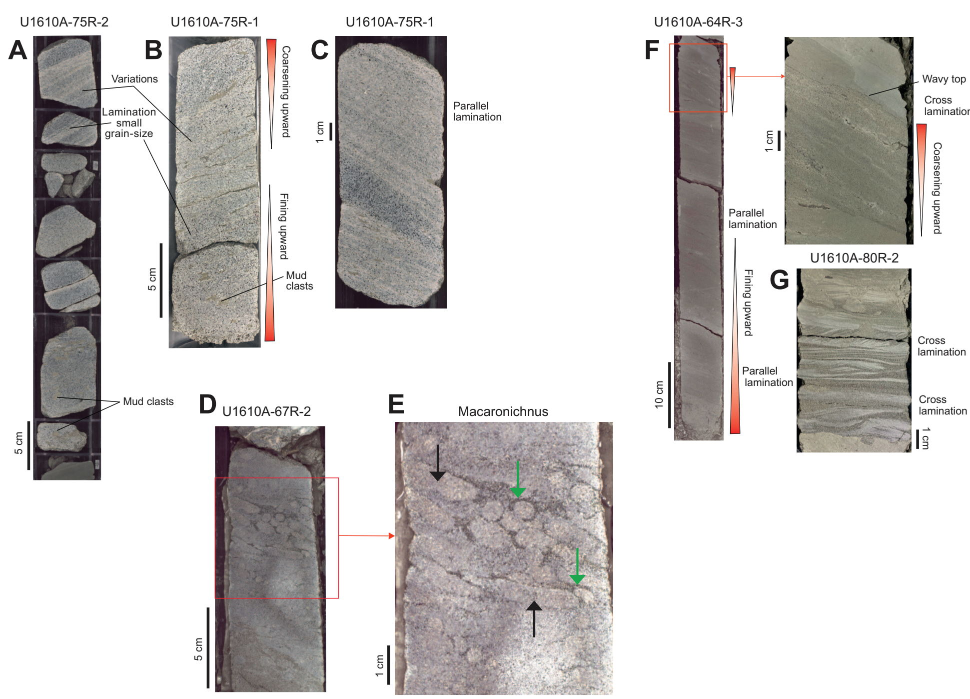

Figure F13. Examples of sandy deposits, Site U1610. A. Lithified sandstones with sharp bases and mud clasts. B. Sandstone with mud clasts, fining-upward interval, and coarsening-upward interval. C. Sandstones with parallel lamination and marked color banding. Dark laminations in C are caused by high proportion of glauconite. D, E. *Macaronichnus* trace fossil (red box in D) and typical mineralogical segregation shown between cylinder tube core (lighter minerals; black arrows) and surrounding rim (darker and heavy minerals; green arrows). F, G. Turbidite deposits with evidence of reworking by bottom currents (F: reworking at top of turbidite; G: stacked sets of cross lamination in turbidite).

both the Guadalquivir Basin and the Deep Algarve Basin during the Messinian and are associated with continental margin progradation, tectonic instability, and relative sea level variations.

Units III and II in the latest Messinian–Early Pliocene (5.78 to >4.52 Ma) have a different depositional style from Unit IV. They comprise hemipelagic deposits and occasional very fine grained turbidites. Unit III and II sediments do not appear to be affected by bottom currents. Based on the interpretation of seismic data, some authors consider MOW to have influenced sedimentation in the Gulf of Cádiz since the Miocene/Pliocene boundary (e.g., Nelson et al., 1999). Others suggest that the earliest Pliocene sediments show no significant MOW activity (e.g., Llave et al., 2011; Expedition 339 Scientists, 2013; Hernández-Molina et al., 2016; van der Schee et al., 2016). However, at Site U1610 it appears that the interval of sedimentation without the influence of MOW occurred earlier than this in the Late Miocene.

During deposition of Unit I later in the Pliocene (4.6–3.57 Ma), bottom water current (contouritic) and pelagic/hemipelagic sediments dominated the succession. Similar Pliocene sequences observed elsewhere in the Gulf of Cádiz are considered to result mainly from MOW bottom currents (e.g., Nelson et al., 1999; Rodrigues et al., 2020).

6.2.3.2. Biostratigraphy

Based on the calcareous nannoplankton and foraminifer assemblage, an age between 3.61 and 3.57 Ma is estimated for the top of the recovered sequence (510.3 mbsf). Below this, a continuous series of calcareous nannoplankton and planktonic foraminifer events are recorded. The presence of *Globorotalia miotumida* and *Reticulofenestra rotaria* at the bottom of the hole constrains the age to Messinian, between 6.38 and ~7.2 Ma (Figure **F12**). The Miocene/Pliocene boundary is placed at ~800 mbsf (the Subunit IIb–IIc transition) based on the HO of *Orthorhabdus rugosus*. However, this bioevent is used with caution because of the scarcity of the specimen in the core catcher (CC) sample analyzed. The next bioevent downcore is the highest common occurrence of *Neogloboquadrina incompta* (sinistral) recorded at ~939 mbsf, which indicates a Messinian age.

During the Pliocene, sedimentation rates determined from biostratigraphy are on the order of ~160 m/Ma and rates are higher during the Miocene, reaching up to 240 m/Ma. The preservation of microfossils is generally good with abundant calcareous nannofossils and planktonic foraminifers, but the concentration and preservation of planktonic foraminifers decline with depth in the Late Miocene samples. The benthonic/planktonic ratio is indicative of intermediate water depths during the Miocene and Pliocene.

6.2.3.3. Paleomagnetism

Paleomagnetism measurements of NRM were performed on all the archive-half core sections from Hole U1610A on the superconducting rock magnetometer (SRM). AF demagnetization was performed at 5, 10, 15, and 20 mT, with measurement of the remaining NRM being taken at a 2 cm resolution after each step. A drilling overprint was mostly removed by 10 mT demagnetization.

In addition, NRM was measured on 134 cube samples on the AGICO JR-6A spinner magnetometer. The samples were then AF demagnetized. The NRM of discrete samples is significantly stronger than at Site U1609, with an average of 10×10^{-4} A/m. In general, steps of 5, 10, 15, 20, 30, 40, 50, 60, and in some cases up to 100 mT were added to fully demagnetize the characteristic magnetic component.

Results from 501 to 540 mbsf clearly show normal inclinations in both the SRM and JR-6A records. Between 540 and 1010 mbsf, reversed directions are dominant and many SRM inclination values approach the expected antipodal GAD inclination at the site (56°). Some short (<20 m) normal polarity depth intervals are present; however, they are not clear, and only a few show successive inclinations with the expected GAD value. Normal polarities dominate from 1010 to 1390 mbsf. Correlations to the GPTS are tentative, but the lack of reversals from 1010 to 1390 mbsf are consistent with the high sedimentation rates observed by biostratigraphy.

We measured the anisotropy of magnetic susceptibility (AMS) and bulk MS of all the discrete samples using the MFK2 KappaBridge instrument. Results show that all the κ_{min} axes have a tilt of ~15°–17° deviating from the vertical. Because κ_{min} is generally perpendicular to the sedimentary bedding plane, this value indicates that drilling was not vertical but must have occurred at an angle of 15°–17°. This is consistent with both the inclined beds in the core and the logging data. In principle, we think it should be possible to reconstruct the strike of the dipping borehole, provided the paleomagnetic signal is robust enough, which will allow AMS results to be interpreted in terms of current flow direction.

6.2.3.4. Geochemistry

In Hole U1610A, the safety protocol for drilling between 740 and 960 mbsf required the methane concentration in headspace gases and methane/ethane ratios to be reported to the drilling team before drilling the next core. For all headspace samples in this interval, the methane concentrations remained <14,000 ppmv (well below the 100,000 ppmv safety threshold), ethane concentrations were <10 ppmv, and the minimum ratio of these two gases (C_1/C_2) was 421. These low concentrations of methane and ethane and the dominance of methane (low C_1/C_2 ratio) presented no concerns for drilling safely because they indicated a microbial rather than petrogenic source. Methane and ethane were commonly detected, whereas ethene, propane, *iso*-butane, and *iso*-propane were detected in trace amounts. Void space was also sampled directly when gas pockets appeared in the core. Although the absolute concentrations were not meaningful, the constituent gases and their relative abundances were comparable to that of the headspace gases and were also indicative of microbial rather than petrogenic sourcing.

Two bottom water samples and 54 IW samples were collected from Hole U1610A for salinity, pH, and alkalinity measurements. One IW sample was collected from every core, except where recovery was limited (<3 m core) or poor quality (abundant fractures), in which case the IW sample was not taken. Approximately 10 mL of IW was extracted initially, which decreased to ~6 mL of water during RCB coring. Sampling continued until water yields decreased below ~1 mL from Core 401-U1610A-61R. An additional IW sample was obtained from Core 72R with insufficient yield for most measurements. Alkalinity ranges 1.4–4.8 mM, pH varies between 7.5 and 8.0, and salinity is 32–35 in IW samples. Major and trace elements in the IW samples were measured by ion chromatography (IC) and inductively coupled plasma–atomic emission spectroscopy (ICP-AES). The bottom water samples each have a salinity of 36, which is elevated relative to ambient Atlantic water and indicates we were sampling MOW.

Overall, $CaCO_3$ ranges 25.4–79.8 wt% with a mean of 35.3 wt% and a standard deviation of 7.3 wt%. Standard reproducibility was 1.12 wt% (n = 13). $CaCO_3$ is generally relatively invariant at Site U1610, with most samples falling within 28–40 wt% downcore. This included some samples selected for color variations, suggesting that color variations are driven by changes in components other than carbonates, likely the siliciclastic fraction.

6.2.3.5. Physical properties and downhole measurements

The upper part of the MS record in Hole U1610A displays 2–7 m thick small-amplitude cycles to 950–1000 m CSF-B where there is a central prominent peak in values with higher amplitude variability. Below this peak, the data are characterized by discrete low-amplitude packages that are 50–100 m thick. A well-defined change at ~700 m core depth below seafloor, Method B (CSF-B) in the NGR data divides higher amplitude regular cycles above and lower amplitude, more variable fluctuations below. Below 1150 m CSF-B, the amplitude and frequency of the cycles increases to the bottom of the hole.

Downhole logging in Hole U1610A unfortunately did not reach deeper than 726 mbsf. Caliper logs show that the hole was alternately washed out to greater than 15 inches and closed into a width narrower than the bit diameter. However, the 220 m long open hole logged interval shows cyclic variation that can be used to cover stratigraphic gaps in Lithostratigraphic Unit I. The density log is strongly affected by borehole conditions, but in narrower borehole intervals the readings are probably valid and reach a maximum of 2.0 g/cm^3. The logging data also quantified the hole inclination, which varied from vertical by 13°–15° in the logged interval. Hole inclination will have to be considered in calculating bed thicknesses and depths to seismic reflectors because coring depth along the borehole overestimates true vertical depth.

The SET2 probe results gave a temperature of 24.8°C at 505.2 mbsf. Using this result and the seafloor temperature of 12°C (measured during the Conductivity-Temperature-Depth tool deployment), the geothermal gradient in Hole U1610A is 25.3°C/km.

6.3. Site U1385

6.3.1. Background and objectives

Site U1385 (37°34.2849′N, 10°7.5616′W) was first drilled during Expedition 339 to provide a marine reference section of Pleistocene millennial climate variability (Figures **F7**, **F14**). Five holes were cored (Holes U1385A–U1385E) to a maximum penetration of 151.5 mbsf using the APC system (Expedition 339 Scientists, 2013). The record extends to 1.45 Ma (Marine Isotope Stage 47) with an average sedimentation rate of 11 cm/ky (Hodell et al., 2015).

Site U1385 (37°34.0128′N, 10°7.6580′W) was reoccupied during Expedition 397 (2022) to deepen the sequence to 400 mbsf, just above the Miocene/Pliocene boundary (~5.3 Ma; Hodell et al., 2023). Five more holes were cored (Holes U1385F–U1385J) ~500 m from the Expedition 339 location with the APC system to about 110 mbsf and the XCB system below that depth (Table **T1**). During Expedition 397, Site U1385 was part of a four site depth transect designed to capture and reconstruct water mass changes during the Pliocene and Pleistocene (Hodell et al., 2023). The two deeper water sites, U1587 and U1586, also recovered Late Miocene successions. Results from Site U1385 demonstrate that the Iberian margin yields long, continuous records of millennial Pliocene–Pleistocene climate variability permitting detailed land–sea comparisons (Hodell et al., 2023).

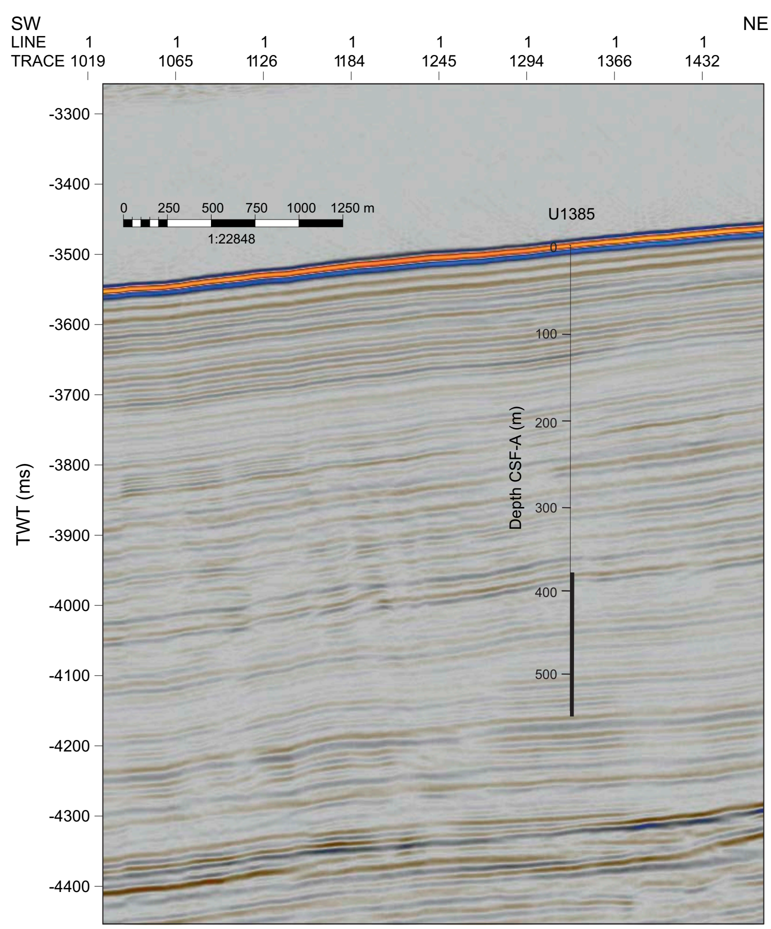

Figure F14. Seismic Profile JC89-9 with location and approximate penetration, Hole U1385K.

Expedition 401 used the same site designation for coring Holes U1385K and U1385L. We distinguish between the intervals recovered by the different expeditions by prefixing the expedition number to the site (i.e., 339-U1385, 397-U1385, and 401-U1385). Site 401-U1385 is located ~20 m from Site 397-U1385 at a water depth of 2590 mbsl, placing it in the NADW (Figure **F2**) (see **Background and objectives** in the Site U1385 chapter [Flecker et al., 2025a]).

6.3.2. Objectives

Extending this remarkable sediment archive back into the Late Miocene was one of the primary goals of reoccupying Site U1385 during Expedition 401. Equivalent aged sediments recovered at the deeper Site U1587 (Hodell et al., 2023) can be traced upslope on the seismic profile to Site U1385. These Late Miocene sediments at Site U1587 display well-developed precessional cyclicity. However, the poor carbonate preservation at this greater water depth (3480 m) means that high-resolution carbonate-based proxy records cannot be generated (Hodell et al., 2023). The shallower water depth of Site U1385 (2590 m) means it is likely to have better carbonate preservation.

Site U1385 is Expedition 401's deepest site. It is located on an elevated ridge, minimizing the chances of disturbance by downslope transport (Figure **F7**). In combination with Site U1609 and the two deeper water Expedition 397 sites, U1587 and U1586, the Late Miocene records from Site U1385 complete a Miocene depth transect equivalent to the Pliocene–Pleistocene transect generated during Expedition 397. The objective was to recover the late Tortonian to Messinian interval at Site 397-U1385 for the following:

- To document the nature, amplitude, and pacing of climate cycles in the Atlantic before, during, and after the MSC and
- To examine water mass variability during this time period, which is characterized by extreme regional changes in oceanographic context.

6.3.3. Operations

Holes U1385K and U1385L were cored after drilling down to start coring a little shallower than the 400 mbsf depth reached at this site during Expedition 397 (Figures **F5**, **F14**).

6.3.3.1. Hole U1385K

The 154 nmi voyage from Site U1610 to Site U1385 took 12.8 h at a speed of 12.0 kt. We lowered the thrusters at 1622 h on 12 January 2024 and switched to dynamic positioning mode at 1652 h. Site U1385 was cored to 151 mbsf during Expedition 339 in 2011 and to 400 mbsf during Expedition 397 in 2022. The APC/XCB BHA was assembled with a PDC bit and lowered toward the seafloor, and a pipe-cleaning pig was pumped down to clean the inside of the drill pipe. The ship was positioned 20 m east of Hole U1385J.

Hole U1385K was started at 0035 h on 13 January and was drilled ahead, reaching 385.0 mbsf at 1615 h. The center bit was retrieved, and we started coring. Cores 2X–6X returned nearly empty, so we ran the bit deplugger to ensure that the bottom of the BHA was free from loose sediment, which may have entered during the preceding drill down. Recovery improved in subsequent cores, and we continued coring through Core 21X at 1035 h on 15 January, having reached the age target of 8 Ma. Cores 2X–21X penetrated from 385.0 to 552.5 mbsf and recovered 127.9 m (76% recovery). We pulled up the pipe, clearing the seafloor at 1328 h on 15 January and ending Hole U1385K.

6.3.3.2. Hole U1385L

The ship was offset 20 m north, and we started Hole U1385L at 1455 h on 15 January 2024, drilling ahead without coring to 376 mbsf. Coring began at 0330 h on 16 January, and Cores 2X–8X penetrated from 376.0 to 443.9 mbsf, recovering 58.4 m (86%). We stopped coring at 1645 h because of the high wind and wave conditions forecast for the evening and next day. The bit cleared the seafloor at 1835 h and was pulled up to a depth of 332 mbsl while the ship began waiting on weather. (After coring Hole U1385K, we had a choice between going directly to the next site or staying to core Hole U1385L; we prioritized collecting core from Hole U1385L, knowing that it would mean waiting on weather the following day.)

The ship began waiting on weather at 2315 h on 16 January. At midmorning on 17 January, the average wind speed reached 35 kt, gusting to 65 kt, and then it eased throughout the day. After waiting on weather for 28.25 h, we were able to resume operations at 0330 h on 18 January. The BHA was raised, disassembled, and stowed. The thrusters were raised at 0720 h, and at 0736 h we started the transit to Site U1611, ending operations at Site U1385.

6.3.4. Principal results

6.3.4.1. Lithostratigraphy

Four lithostratigraphic units are defined at Site U1385, and they are characterized by alternating light-colored (light greenish gray) and dark-colored (greenish gray and gray) beds composed of clayey calcareous ooze and calcareous clay with lighter and darker shades and gradational and sharp boundaries (Figures **F15, F16**). Minor lithologies include clay- and pyrite-rich intervals and horizons exhibiting multiple hues, including shades of orange-brown and blue-green. Trace fossils include *Chondrites, Planolites, Thalassinoides*, and *Zoophycos*, as well as rare *Asterosoma, Palaeo-*

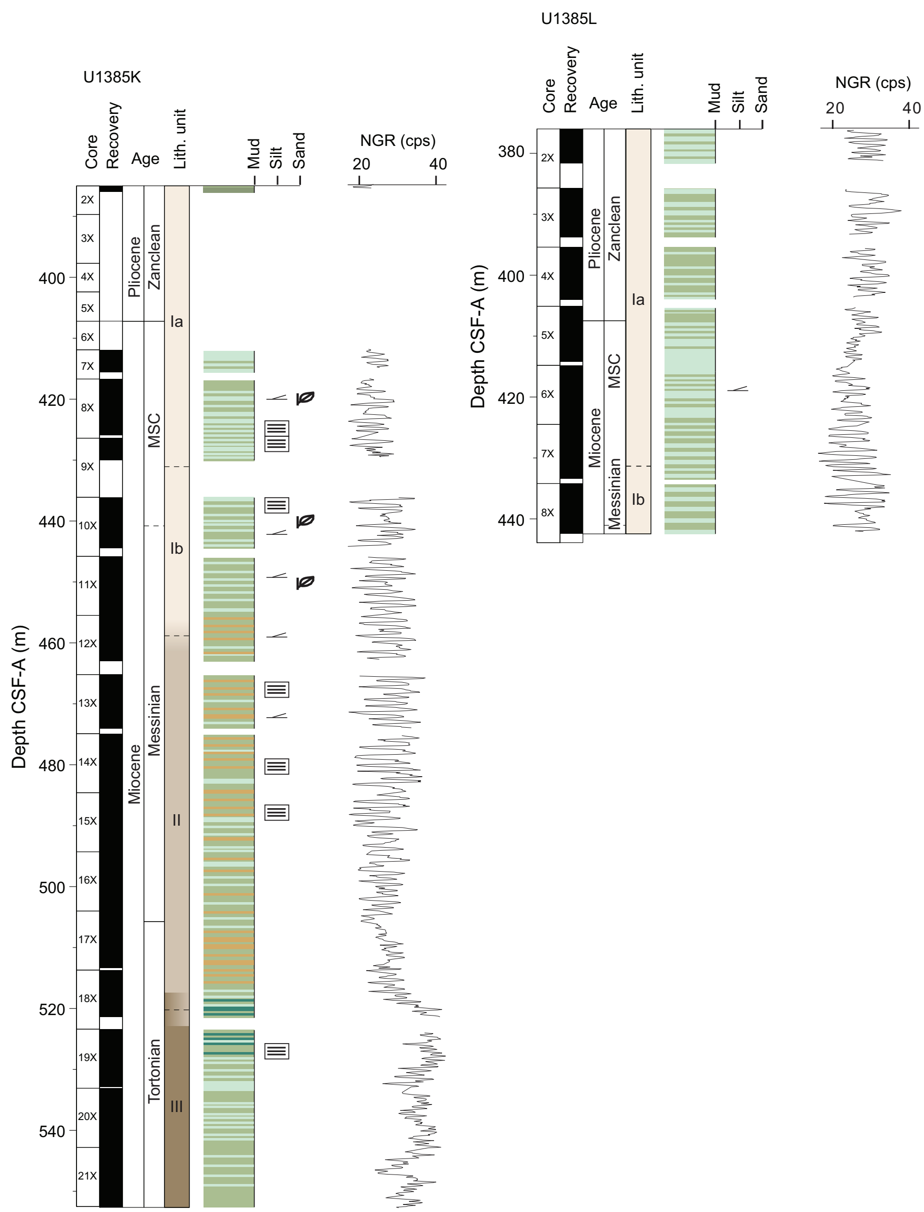

Figure F15. Site U1385 synthesis. See Figure F6 for lithology and symbol legend. cps = counts per second.

phycus, and *Schaubcylindrichnus*. Pyrite nodules and shell fragments are disseminated throughout. Sediments are initially interpreted to be deepwater hemipelagic deposits.

Unit I extends from 385.0 to 458.5 mbsf in Hole U1385K and from 376 to 442.5 mbsf in Hole U1385L. It comprises clayey calcareous ooze (light greenish gray) and calcareous clay (greenish gray). It consists of two subunits; Subunit Ia (385.0–430.0 mbsf in Hole U1385K and 376.0–430.5 mbsf in Hole U1385L) consists of more homogeneous sediments than Subunit Ib (430.0–458.5 mbsf in Hole U1385K and 430.5–442.5 mbsf in Hole U1385L), which contains sharp contacts between calcareous clay and clayey calcareous ooze. Unit II extends from 458.5 to 519.6 mbsf in Hole U1385K and includes frequent cyclic alternations between calcareous clay (dark gray and olive-gray) and clayey calcareous ooze. Unit III extends from 519.6 to 552.65 mbsf in Hole U1385K

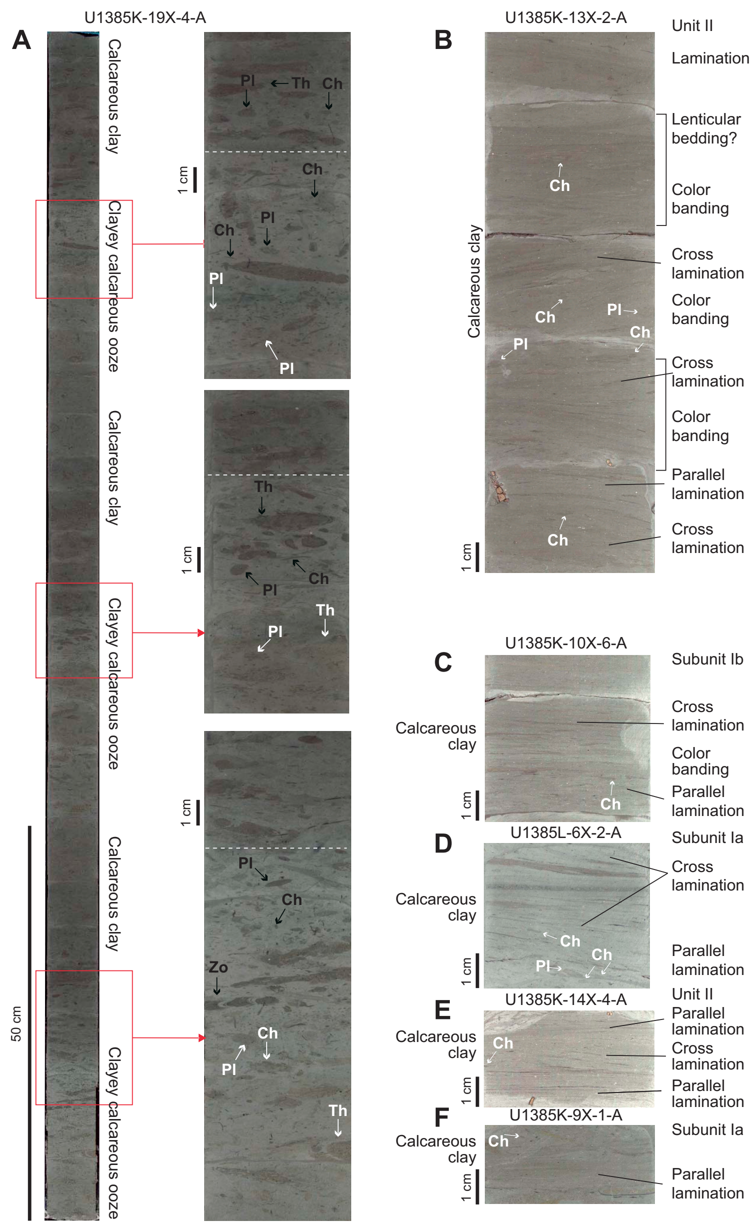

Figure F16. Examples of sedimentary structures, Site U1385. A. Alternating lithologies showing regular sedimentary cycles between calcareous clay (darker facies) and clayey calcareous ooze (lighter facies), with detail of trace fossils in contact (dashed white line) between facies. Note differentiation between dark (black arrows) and light (white arrows) trace fossil assemblages and penetration of dark traces into lighter sediments. B–F. Color banding, parallel lamination, cross lamination, and lenticular bedding associated with calcareous clay. Ch = *Chondrites*, Pl = *Planolites*, Th = *Thalassinoides*, Zo = *Zoophycos*.

and predominantly consists of calcareous clay (dark gray and olive-gray) with thinner beds of clayey calcareous ooze.

Site U1385 is located on a plateau (Promontório dos Príncipes de Avis) below the water depth of the present-day Mediterranean outflow plume (Figure **F2**). This area is protected from sedimentary input from slope deposition or submarine canyons. The Miocene sediments recovered from Site U1385 are dominated by pelagic clayey calcareous ooze and calcareous clay deposits, consistent with this setting. Precessional-scale variability in the Miocene and late Tortonian sediments recovered may have resulted from fluctuations in carbonate and/or siliciclastic input, generating pelagic deposits with color-carbonate cycles. This may be driven either by local climatic variability or result from nepheloid layers higher in the water column (e.g., associated with MOW) (Abrantes, 2000; Ambar et al., 2002; Magill et al., 2018) containing significant quantities of suspended sediment.

Future research will evaluate the influence of regional water masses on the dominant pelagic sedimentation at Site U1385. The interplay between NADW and Antarctic Bottom Water (Figure **F2**) (van Aken, 2000; Hernández-Molina et al., 2011; Glazkova et al., 2022) would have been particularly important during the latest Miocene when Atlantic intermediate and deepwater circulation evolved into a pattern similar to the one observed today (Sykes et al., 1998; Billups, 2002; Nisancioglu et al., 2003; Uenzelmann-Neben et al., 2017; Hernández-Molina et al., 2017).

6.3.4.2. Biostratigraphy

Calcareous nannofossils are typically abundant with moderate and good preservation, and planktonic foraminifers are well preserved with evidence of fragmentation in only a few samples. The age of the succession is constrained by eight nannofossil events and four foraminifer events. The HO of *O. rugosus* (5.23 Ma) and the lowest occurrence of *Ceratolithus acutus* (5.36 Ma) are recorded between Sections 401-U1385L-4X-CC and 5X-CC at ~409 mbsf, constraining the Messinian/Pliocene boundary to Core 5X (Figure **F15**). The oldest bioevent identified is the base of the paracme of *Reticulofenestra pseudoumbilicus* (8.8 Ma) between Sections 401-U1385K-19X-CC and 20X-CC at ~517 mbsf. Core catcher samples were also analyzed for benthonic foraminifer content; the assemblage seems well preserved.

6.3.4.3. Paleomagnetism

Pass-through paleomagnetic measurements were performed on the SRM to investigate the NRM on a total of 132 archive-half sections (91 sections from Hole U1385K and 41 sections from Hole U1385L). AF demagnetization was performed on the SRM by applying stepwise peak fields of 5, 10, 15, and 20 mT, with measurement of the remaining magnetization taken at a 2 cm resolution. In addition, we collected and measured 117 discrete samples of the working-half sections, using 3–7 discrete samples from each core. First, the AMS and bulk MS were measured on all samples using the MFK2 KappaBridge instrument. Next, the NRM of 61 cube samples (47 samples from Hole U1385K and 14 samples from Hole U1385L) was measured on the AGICO JR-6A spinner magnetometer. Stepwise AF demagnetization was performed at successive peak fields of 0, 5, 10, 15, 20, 30, 40, 50, 60, and 70 mT, up to a maximum of 80 mT for samples from Hole U1385K and a maximum of 40 mT for samples from Hole U1385L where the magnetic signal was weaker. When magnetization became erratic, demagnetization was stopped.

Constrained by stratigraphic correlation to Hole U1385J, the topmost core of Hole U1385L is <5 Ma. We then correlated the reversal pattern in inclination values of SRM measurements after 20 mT and JR-6A measurements after 20 mT to the most recent GPTS. Based on this magnetostratigraphy, the base of Hole U1385K is slightly older than 8.2 Ma and the average sediment accumulation rate is ~5 cm/ky for the Messinian part of the record.

The AMS results of Holes U1385K and U1385L show an overall vertical direction of the κ_{min} axis, which is in agreement with a horizontal sedimentary fabric and a vertically drilled hole.

6.3.4.4. Geochemistry

For Hole U1385K, one headspace gas sample and IW sample were taken per core. Gas content in Hole U1385K was within the safety range; only methane (<24,000 ppmv) and ethane (<1 ppmv) were detected in the top sample with lower levels of methane only below. IW samples from Hole

U1385K were measured for salinity, pH, and alkalinity. Salinity remained invariant at 32 throughout the cored interval. IW major and trace elements were measured by IC and ICP-AES. IW profiles were compared to earlier drilling of shallower stratigraphy in Expedition 397 Hole U1385G, yielding useful context and showing some analytical discrepancies between the data generated by the two expeditions. Sediment samples were obtained from the IW squeeze cake residues in Hole U1385K and one sample per core from Hole U1385L to understand geochemical variations. TOC is <1% and TN is <0.05%. The C/N ratio mean is 14 with a standard deviation of 13, indicating that the organic carbon is dominantly of marine origin with sporadic input of terrestrial organic matter. There is no significant downhole trend in the data, suggesting that marine production and terrestrial inputs as well as organic degradation are broadly consistent across the drilled interval, with variability likely cyclic at frequencies higher than that sampled here. Calcium carbonate abundance varies from 39 to 69 wt% and correlates well with NGR, showing that mixing of carbonate and siliciclastic fractions is controlling the observable cyclicity at this location. Carbonate geochemistry shows lithology-dependent variations and signs of carbonate diagenesis.

6.3.4.5. Physical properties and downhole measurements

The full suite of physical properties measurements was made on cores and samples from Holes U1385K and U1385L. Moisture and density measurements show a compaction trend with depth: bulk density increases from ~1.9 g/cm^3 at 378 mbsf to 2.0 g/cm^3 at 548 mbsf, and porosity decreases from 50% to 43% over the same depth interval. NGR and MS records contain cyclic alternations on a meter to submeter scale throughout the cored interval (Figure **F15**), with higher amplitude cycles from ~420 to 505 mbsf relative to the lower part of the core. No downhole measurements were made at Site U1385.

6.4. Site U1611

6.4.1. Background and objectives

Site U1611 (proposed Site WAB-03A) is located in the Mediterranean just east of the Gibraltar Strait in the Alborán Sea (Figure **F17**) (see **Background and objectives** in the Site U1611 chapter [Flecker et al., 2025d]). It marks the eastern end of Expedition 401's transect of sites that track MOW from its source, through the Atlantic–Mediterranean gateway into the Gulf of Cádiz (Site U1610), and around to the west of the Iberian margin (Sites U1609 and U1385) (Figure **F2**). Today, the Alborán Basin is a relatively narrow (150 km wide, north to south), shallow (maximum depth = 1800 m), elongate (350 km long, east to west) area that links the deeper parts of the Mediterranean Sea to the Atlantic. Atlantic water flows into the Mediterranean through the Gibraltar Strait at the surface as a coherent layer of warm and relatively fresh marine water, whereas deeper, cooler, and more saline water generated in the Mediterranean flows through the Alborán Sea and

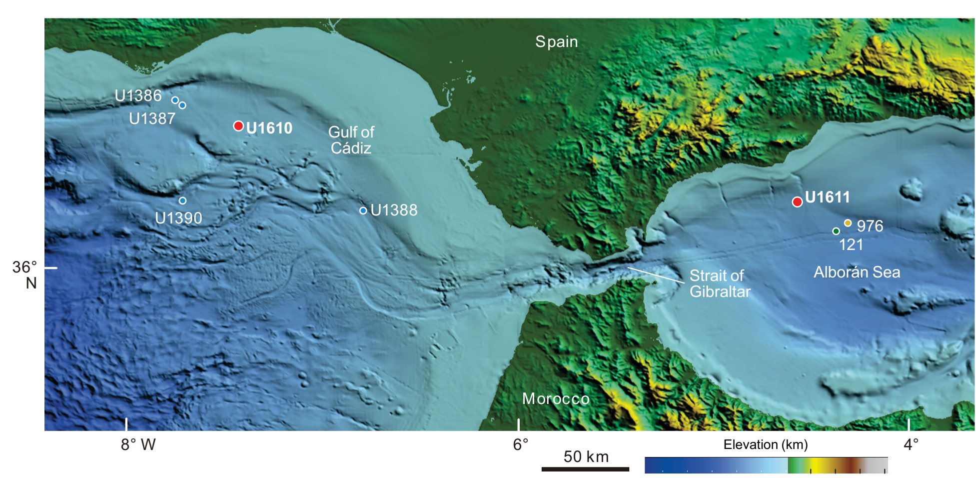

Figure F17. Bathymetric map of Gulf of Cádiz and Alborán Sea showing Sites U1610 and U1611 in relation to previously drilled sites in the area. See Figure F1 for legend.

out into the Atlantic at depth (Figure **F18**). The stratified water mass structure in the Alborán Sea reflects this exchange, as well as the densities of the different water masses generated within the Mediterranean, principally the Levantine Intermediate Water and Western Mediterranean Deep Water (WMDW) (Ercilla et al., 2016) (Figure **F2**). Site U1611 is located on the north side of the basin on the Spanish continental slope at a water depth of 810 mbsl (Figure **F17**). Today, this area is bathed in WMDW with a temperature of ~12.9°C and a salinity of ~38.45 (Figure **F19**). It is directly impacted by westward flowing currents that produce contourite deposition along the Spanish margin (Figure **F18**) and by receiving the input of gravity deposits from upslope (Ercilla et al., 2016).

Exchange through a single gateway at Gibraltar is a relatively recent (Pliocene–Pleistocene) phenomenon (Hernández-Molina et al., 2014a; van der Schee et al., 2016; García-Gallardo et al., 2017a; Flecker et al., 2015). As a result of Africa-Eurasia convergence, westward docking of the Alborán plate, and simultaneous slab retreat (Jolivet and Faccenna, 2000; Faccenna et al., 2004; van

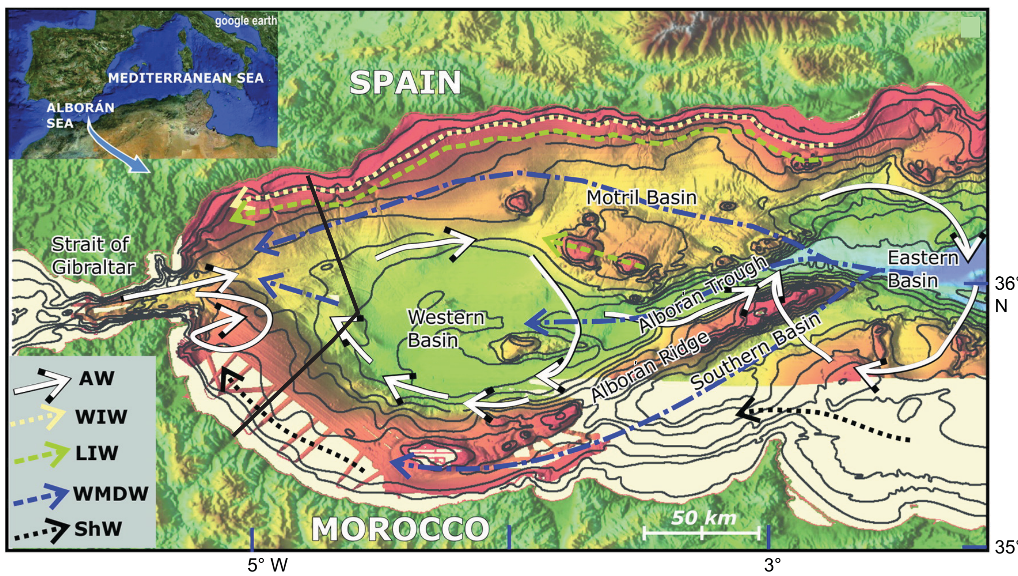

Figure F18. Bathymetric map of Alborán Sea with present-day water masses and currents. AW = Atlantic Water, WIW = Western Intermediate Water, LIW = Levantine Intermediate Water, WMDW = Western Mediterranean Deep Water, ShW = shelf water (mix of AW and WMDW). (Figure from Ercilla et al., 2016.)

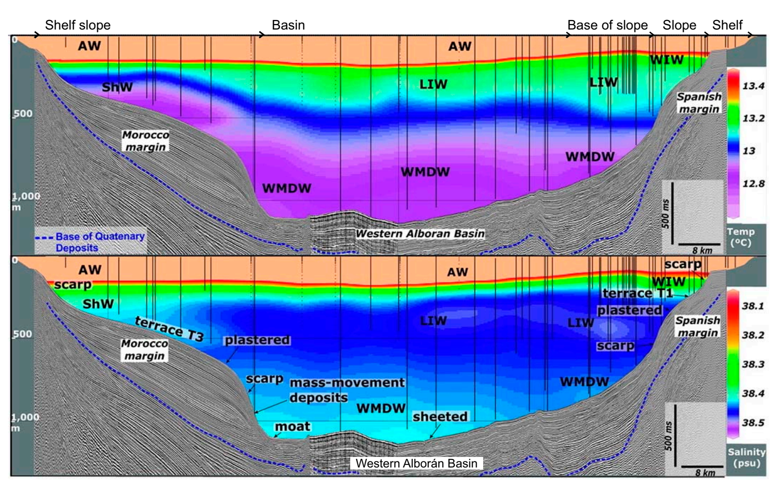

Figure F19. Water mass structure, Alborán Sea (Ercilla et al., 2016). AW = Atlantic Water, WIW = Western Intermediate Water, LIW = Levantine Intermediate Water, WMDW = Western Mediterranean Deep Water, ShW = shelf water (mix of AW and WMDW).

Hinsbergen et al., 2014), the Atlantic–Mediterranean connection evolved from a single, wide open seaway in the Tortonian (Figure **F3**) linking a Mediterranean that was more of an embayment of the Atlantic than a distinct marginal marine system (Flecker et al., 2015) to two narrow corridors in the early Messinian: one in northern Morocco and the other in southern Spain (Figure **F20**) (Martín et al., 2014).

Ongoing restriction of the marine corridors permitted Mediterranean salinity to rise, and a distinct, dense water mass formed. Ultimately, the narrowing and closure of these connections resulted in extreme salinity fluctuations in the Mediterranean, leading to the precipitation of more than 1 million km^3 of salt, equivalent to ~6% of the total dissolved oceanic NaCl (Blanc, 2006; Ryan, Hsü, et al., 1973) in the latest Miocene. This event is known as the MSC (Hsü et al., 1973). Progressive tectonic convergence coupled with isostatic rebound related to lithospheric mantle dynamics (Duggen et al., 2003) not only severed these earlier marine connections but also uplifted and exposed them on land (Capella et al., 2017). In the Early Pliocene, two-way exchange was established through a single conduit, the Gibraltar Strait. This reconnection event is known as the Zanclean deluge. Many authors suggest that catastrophic failure of the Atlantic/Mediterranean barrier at Gibraltar led to the swift refilling of the Mediterranean Sea associated with major erosion in the Alborán Basin (Estrada et al., 2011; Lofi, 2018; Garcia-Castellanos et al., 2020).

6.4.2. Objectives

Site U1611 targets one of the few thick late Messinian sedimentary successions in the Alborán Basin. The record recovered from this location provides key constraints on the chemistry and physical properties of MO during the Late Miocene. The major objective for Site U1611 was to recover an 8–4 Ma succession that records the evolution of the Alborán Sea before, during, and after the MSC. This information will then be used to test the following hypotheses:

- The Alborán Basin was an intermediate marine system influenced by the Atlantic and separated from the Mediterranean by the Alborán volcanic arc during the MSC.

Figure F20. Schematic maps showing closure and opening of Mediterranean–Atlantic gateways from late Tortonian to Zanclean (updated after Martín et al., 2014).

- Mediterranean–Atlantic exchange occurred through the Gibraltar Strait before the start of the MSC.
- Extreme environmental fluctuations in the Mediterranean are mirrored by both environmental conditions in the Alborán Sea and visible perturbations down the MO plume in the Atlantic.

6.4.3. Operations

On the morning of 19 January 2024, *JOIDES Resolution* sailed through the Strait of Gibraltar, one of the Mediterranean–Atlantic gateways in the title of Expedition 401. The 333 nmi transit from Site U1385 to Site U1611 in the Alborán Basin of the Mediterranean Sea took 29.8 h at an average speed of 11.2 kt. We arrived on site at 1315 h on 19 January, lowered the thrusters, and started to unstow the BHA. At 1745 h, high winds made it unsafe for the derrickman to work at the monkey board in the derrick, so we waited until 2015 h for the wind to drop before resuming operations (a 2.5 h delay).

The rig floor team assembled ~650 m of 10¾ inch casing, hung it below the ship, and made up the casing stinger BHA, including the bit, underreamer bit, and mud motor. The BHA and drill pipe were lowered through the casing until the bit and underreamer extended below the casing by 3 m. The HRT running tool was attached to the casing, and the funnel was welded on. The funnel was lowered through the moonpool at 1540 h, and the entire casing system was lowered to 792.1 mbsl before installing the top drive. Hole U1611A was started at 1730 h, and we continued to drill the casing into Hole U1611A until the reentry cone base landed on the seafloor at 810.1 mbsl with the bit at 654.6 mbsf and the casing shoe at 652.6 mbsf. The subsea camera was deployed to observe the release of the casing, and at 0405 h on 22 January the casing assembly was released from the pipe and BHA. The bit was raised back to the ship, clearing the rig floor at 1103 h and completing the casing portion of operations in Hole U1611A. The RCB BHA was then assembled with a PDC bit and lowered to 584.9 mbsl, and the subsea camera was deployed again to guide reentry into the hole.

Hole U1611A was reentered at 1832 h, and the top of the cone was confirmed to be at 807.3 mbsl with the seafloor at 810.1 mbsl, very close to the PDR estimate of seafloor depth at 810.2 mbsl. The bit was lowered down the casing to 613 mbsf, where it took weight, probably because it met sediments that had come up into the casing. The top drive was installed, and the bit was washed down to 656.3 mbsf, followed by a 30 bbl mud sweep to clear any remaining loose sediment from the casing. At 0000 h on 23 January, the core line winch electrical controller failed, specifically the Veeder-Root counter in the controller. It was replaced, and the winch was back online by 0545 h. The first run on the core line was the SET2 tool. The Icefield MI-5 core orientation tool, usually run to orient APC cores, was run by piggybacking on the SET2 tool deployment to estimate any deviation of the casing from vertical. It showed a small angle at the top of the casing, deviating to 10° at the base of the casing. This result was subsequently confirmed by the downhole logging inclinometer data. Coring started at 0815 h with Core 2R; however, it recovered only 3 cm of sediment, so we ran the bit deplugger. Recovery improved for subsequent cores. Cores 2R–24R penetrated from 656.3 to 879.4 mbsf and recovered 223.1 m (74%). Cores 25R and 26R returned nearly empty, probably because coarse-grained sediments in the formation entered the base of the pipe. The bit deplugger was deployed again. We made five 30 bbl mud sweeps per day to flush cuttings and loose sediment out of the borehole, and coring continued with moderate to good recovery. At 0815 h on 26 January, following Core 44R, we switched to half-core advances, which improved core recovery (on 26 January full-core advances yielded 69% recovery and half-core advances yielded 87%).

We switched from half-length to full-length RCB core advances with Core 401-U1611A-77R. Core 79R returned empty, so we ran the bit deplugger again and switched back to half-length advances for Cores 80R–83R, each of which recovered less than 10 cm. Because hole conditions were difficult, at 1945 h we started a wiper trip to clear bridges in the hole prior to further coring and downhole logging. Overpulls of 20,000–30,000 lb were observed at 1104.9, 949.4, 881.7, and 872.0 mbsf before the bit could be raised to the casing shoe. On washing down, 12 tight spots were encountered and 6 m of fill was found at the base of the hole. From 0730 to 1030 h on 29 January, we washed out the fill and swept the hole with 30 bbl sepiolite mud in preparation for coring. Cores

84R–86R penetrated to 1281.9 mbsf, the final depth of the hole, and recovered 13.2 m (68%). Cores 2R–86R penetrated from 656.3 to 1281.9 mbsf and recovered 431.2 m of core (69%).

At 1545 h, we started to prepare the hole for downhole logging. The bit was released at the base of the hole, the hole was displaced with barite-weighted mud, and the end of the pipe was raised to 672.7 mbsf. The rig floor team assembled the triple combo logging tool string, without the source, and started lowering it down the pipe at 2145 h. The tool string reached an impassable obstruction at 909.6 mbsf and made a repeat and main pass, which together cover the open hole interval from 672.7 to 909.6 mbsf. Borehole diameter varied between narrower than 6 inches to wider than the maximum extent of the caliper measurement (17 inches), and the logged interval of the borehole was inclined from the vertical by between 10° and 15°. The triple combo tool string was back on deck at 0410 h on 30 January, and a sonic-inclinometry tool string was assembled for the second logging run. This tool string was lowered into the borehole but could not pass below 743.6 mbsf. It recorded data for the short interval up to the bit and was back on deck by 0910 h, and the logging equipment was disassembled by 1100 h. The BHA was raised back to the ship, clearing the rotary table at 1400 h and ending Hole U1611A. A new mechanical bit release and PDC RCB bit were added to the BHA and lowered back down close to the seafloor.

The ship was offset 1316 m northwest, and Hole U1611B was started at 1725 h on 30 January at a water depth of 784 mbsl. The relatively large offset was made to core part of the seismic profile where reflectors had greater horizontal continuity than in Hole U1611A (Figure **F21**). We drilled ahead to 744.9 mbsf and pumped 30 bbl sepiolite mud sweeps after adding every two stands of pipe to keep the hole clear. When the center bit was retrieved, 1.7 m of sediment was found behind it in the core barrel, which was curated as a wash core (2W). Coring started at 1830 h on 31 January. Cores 3R and 4R had 91% recovery, but the following two cores, 5R and 6R, returned nearly

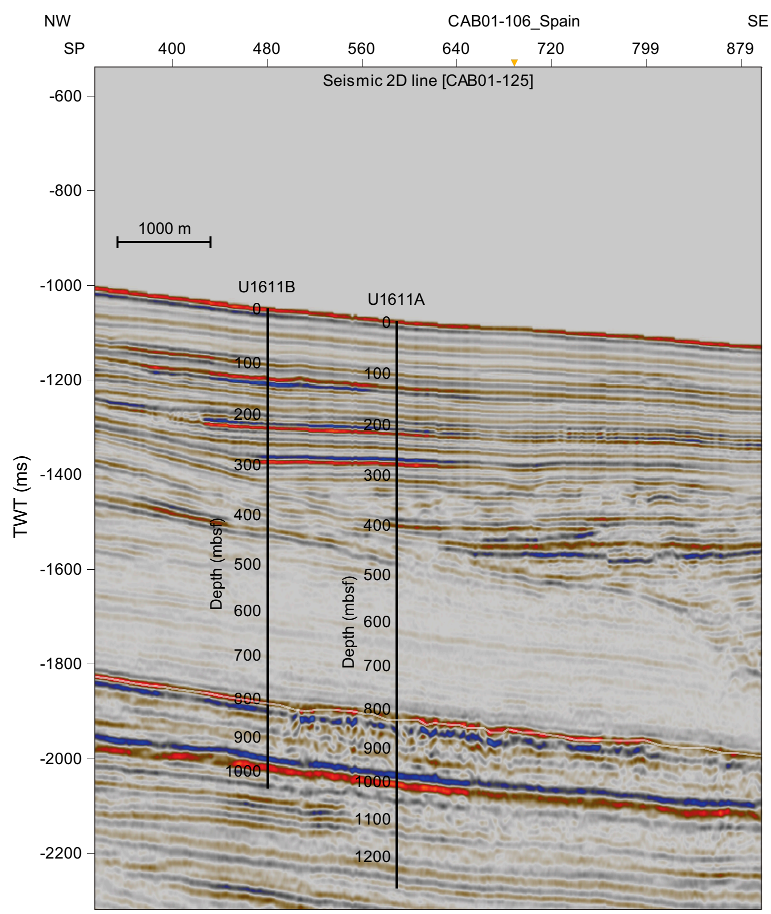

Figure F21. Seismic Profile CAB01-125 with location and approximate penetration, Holes U1611A and U1611B. SP = shot-point.

empty, so we ran the bit deplugger and then switched to half-core RCB advances. Coring proceeded with half-core advances for the next 3 days until operations needed to stop to start preparing for the transit to Napoli, Italy. Core 66R arrived on the catwalk at 2330 h on 4 January and was the last core of the site and the expedition. Cores 3R–66R penetrated from 744.9 to 1069.9 mbsf and recovered 255.1 m (78%).

6.4.4. Principal results

6.4.4.1. Lithostratigraphy

Four main lithologies were described at Site U1611: (calcareous) mud, (calcareous) silty mud, sandy silt, and silty sand. Minor lithologies include sandy mud, conglomerate, breccia, and cemented carbonate (e.g., dolostone and limestone). On the basis of lithologic changes, Holes U1611A and U1611B are divided into three lithostratigraphic units (Figure **F22**). Contacts between these units and the lithologies within them are mainly gradational in Unit I (Early Pliocene), characterized by subtle changes in color and grain size, and become more commonly sharp in Units II and III (Messinian), associated with distinct color changes and frequent laminations. The coarser silts and sandier beds typically have sharp to erosive basal contacts.

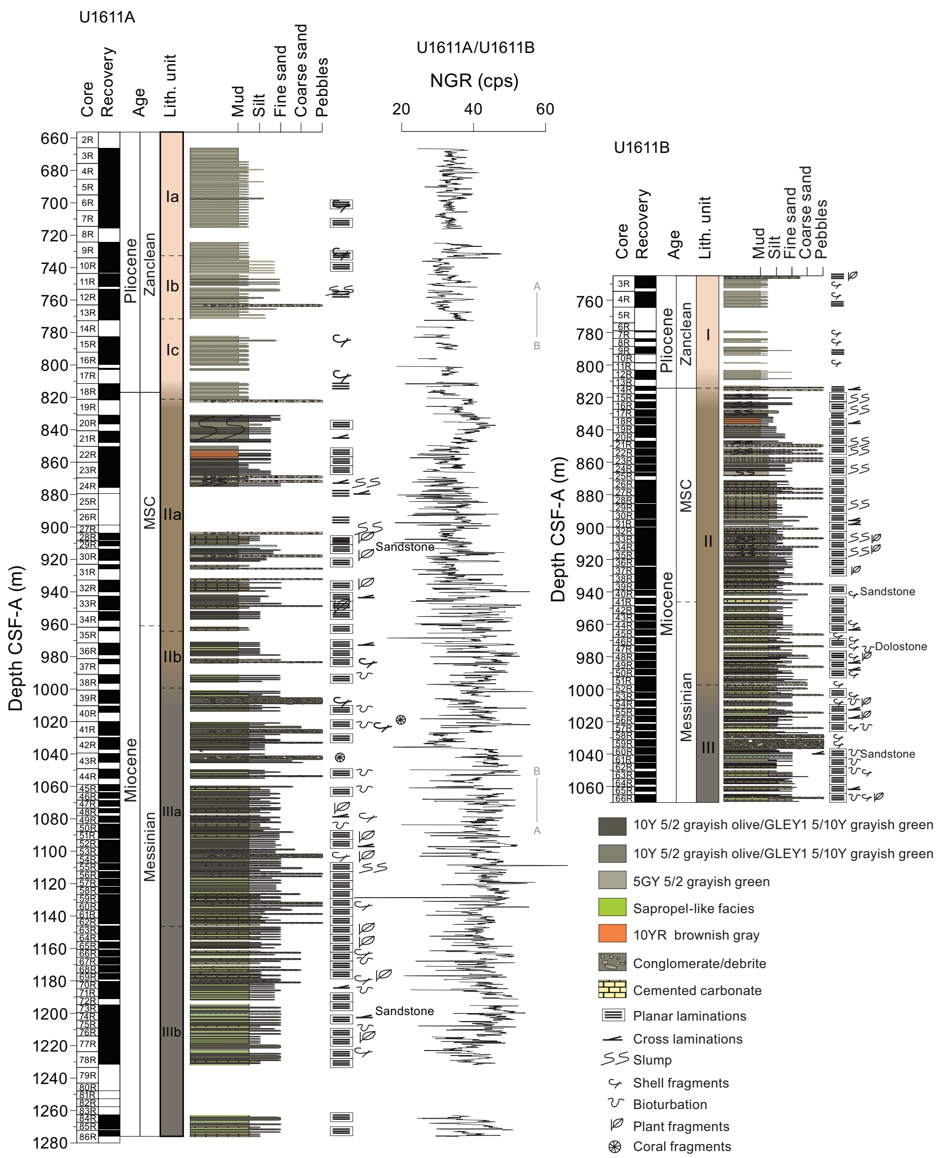

Figure F22. Site U1611 synthesis. NGR data shown are derived mainly from Hole U1611B, with upper and lower intervals from Hole U1611A. Labeled vertical lines = transition between hole NGR data sets. cps = counts per second.

Unit I extends from 656.3 to 820.4 mbsf in Hole U1611A and from 746.4 to 814.2 mbsf in Hole U1611B. In Hole U1611A, Unit I comprises three subunits, all consisting of alternating calcareous mud and calcareous silty mud. Subunit Ib (733.9–772.3 mbsf) contains more occurrences of coarser lithologies including conglomerates and calcareous sandy silt compared to Subunits Ia (656.3–733.9 mbsf) and Ic (782.4–820.4 mbsf) (Figure **F23**). In Unit I in Hole U1611B, calcareous muds also alternate with calcareous silty muds, with the frequency of coarser lithologies increasing with depth.

Unit II extends from 820.4 to 996.5 mbsf in Hole U1611A and from 814.2 to 996.9 mbsf in Hole U1611B. In Hole U1611A, it is characterized by the presence of laminated beds alternating with nonlaminated and sometimes coarser grained beds. Unit II consists of two subunits. Subunit IIa (820.4–964.3 mbsf) is composed of lithologies with variable carbonate content, including mud, calcareous mud, calcareous silty mud, sandy silt, and silty sand, with minor aragonite, cemented carbonate, breccia, and conglomerate (Figure **F23**). Subunit IIb (971.5–996.5 mbsf) is composed of lithologies similar to those in Subunit IIa, but with a lower carbonate content, with beds of calcareous muds and calcareous silty muds alternating with muds, sandy silts, and sands. In Hole U1611B, Unit II mostly consists of the same lithologies as those in Hole U1611A, typically with a lower calcareous content with increasing depth. However, in Hole U1611B, more silty muds were described in the deeper part of Unit II, and in general, coarser beds are more common.

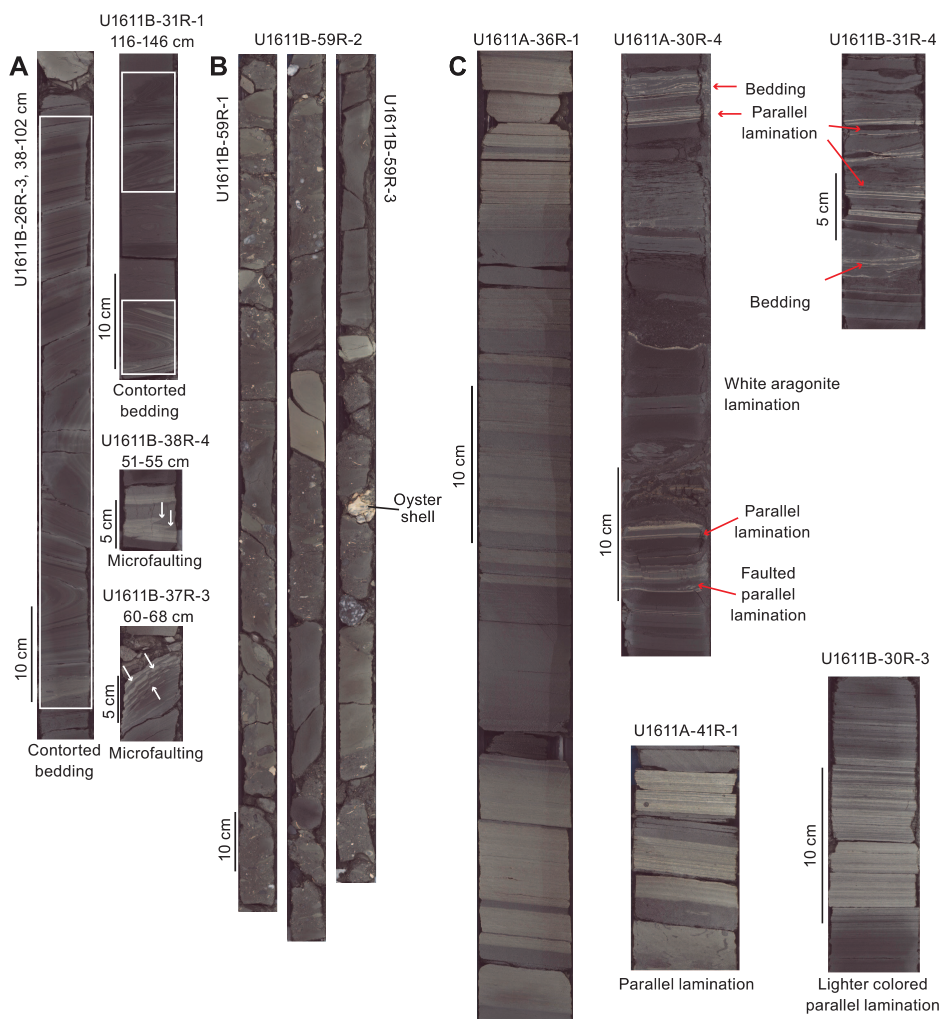

Figure F23. Linescan images of deformational and laminated structures. A. Contorted bedding (slump), microfaulting, and chaotic deposits. B. Conglomerate >1 m long with mud clasts and large bioclasts. C. Examples of lighter colored laminations reflecting variable carbonate content (401-U1611A-36R-1 and 401-U1611B-30R-3), white lamination composed of aragonite that are parallel (401-U1611A-30R-4 and 401-U1611B-31R-4), and deformed (contorted and faulted) parallel and cross lamination (401-U1611A-41R-1).

Unit III extends from 1000.6 to 1275.9 mbsf in Hole U1611A and from 997.1 to 1069.69 mbsf in Hole U1611B. In Hole U1611A, Unit III consists of two subunits. Subunit IIIa (1000.6–1144.9 mbsf) consists of frequent alternations of silty mud and calcareous silty mud in the shallower parts, with numerous intervals of sandy silt and silty sand. The proportion of calcareous silty mud is lower in the deeper part of Subunit IIIa. There is also minor conglomerate typically associated with contorted, slump-like sediment deformation, and cemented carbonate. Subunit IIIb (1146.1–1275.9 mbsf) consists of similar lithologies to Subunit IIIa, except that Subunit IIIb lacks the rapid interbedding of calcareous silty mud and silty mud and contains more frequent occurrences of coarser grained intervals (e.g., sandy silt and silty sand). In Hole U1611B, Unit III is similar to the upper part of Subunit IIIa in Hole U1611A, except that there is a notable thick conglomerate (8.5 m) that was not recovered in Hole U1611A. Unit III is characterized by the presence of laminated beds alternating with nonlaminated and normally graded beds, but the lamination appears subtler than in Unit II (Figure **F23**).

During the Messinian, particularly in Unit III, there is evidence of an interplay of gravitational and pelagic/hemipelagic processes. This produced a complex depositional system in which the slumps, debrites, and turbiditic deposits are volumetrically the most important deposits in the succession, resulting in a high sedimentation rate. Unit II is characterized by the development of lamination throughout, along with the presence of thin aragonite layers, dark muds, and so on. During this time, the basin likely became more restricted, and the relatively high sedimentation rate and low bottom water oxygenation led to a benthonic-poor habitat, limiting the macrobenthos trace-fossil maker community sufficiently to prevent bioturbation and preserve the finely laminated sediments (Schimmelmann et al., 2016). These processes and the precipitation of aragonite are possible in stratified marine lakes with restricted seawater access and water column stratification (Schimmelmann et al., 2016). Turbidite and debrite deposits are also present in Unit II, and according to the literature on this sector of the Alborán Sea, these deposits are considered to be chaotic mass transport deposits that accumulated during the MSC (Martínez del Olmo and Comas, 2008; Estrada et al., 2011; Martínez del Olmo, 2011; Bulian et al., 2021). Based on the results from this expedition, Unit II has thinner and finer gravitational deposits that occur less commonly than in Unit III.

The Pliocene sediments in Unit I display clear evidence of bottom water currents (contouritic) and pelagic/hemipelagic sedimentation. Similar Pliocene sequences observed elsewhere in the Alborán Basin are considered to result mainly from the regional circulation of the deep, intermediate, and surface Mediterranean water mass currents (e.g., Juan et al., 2016, 2020; Ercilla et al., 2016; Llave et al., 2020). The transition from the low-oxygen finely laminated sediments of Unit II to the well-oxygenated contouritic sediments of Unit I occurs over a ~2 m interval that was not recovered in either Hole U1611A or U1611B. Dating of the uppermost Miocene and lowermost Pliocene sediments on either side of this recovery gap is necessary to determine the duration of this transition, which may be associated with the catastrophic refilling of the Mediterranean at the Miocene/Pliocene boundary (Garcia-Castellanos et al., 2020).

6.4.4.2. Biostratigraphy

This site is characterized by some intervals poor in microfauna, particularly planktonic foraminifers. However, despite some core catchers being barren of foraminifers, they were rich in fish teeth and scales, wood fragments, and shell fragments, providing valuable information about the site's paleoenvironment.

Both holes were designed to start retrieving cores from the Early Pliocene, and this age was confirmed by the calcareous nannoplankton and foraminifer assemblages recovered in the uppermost core catcher samples (656 mbsf in Hole U1611A and 744 mbsf in Hole U1611B). Below Samples 401-U1611A-18R-CC (821.2 mbsf) and 401-U1611B-14R-CC (815.7 mbsf), close to the Lithostratigraphic Unit I/II boundary, planktonic foraminifers are absent (with rare exceptions) in the fraction larger than 150 µm, although they continue to be present in the 63–150 µm fraction. We interpret this change to be the Messinian/Zanclean boundary. There is also a significant change in the composition of the sediments below this boundary, with almost no biogenic particles in the coarse fraction except for fish and wood fragments. The near total absence of >150 µm planktonic foraminifers continues to Sample 401-U1611A-42R-CC (1037.2 mbsf). Below this sample to the bottom of Hole U1611A, the sediments typically contain some planktonic foraminifers in the >150 µm fraction but few benthonic foraminifers. The presence of calcareous nannofossils *R. pseudoumbilicus* and *Nicklithus amplificus* in the lowermost sample from Hole U1611A (1281.9 mbsf) constrains the age at the base of the hole to the late Messinian younger than 6.82 Ma (Figure **F22**).

6.4.4.3. Paleomagnetism

Pass-through paleomagnetic measurements were performed on the SRM to investigate the NRM of all the archive-half sections of Holes U1611A and U1611B. AF demagnetization was performed on the SRM by applying stepwise peak fields of 5, 10, 15, and 20 mT, with measurement of the remaining magnetization taken at a 2 cm resolution.

In addition, we collected discrete samples from all the working-half sections of Hole U1611A. We measured the AMS and bulk MS using the MFK2 KappaBridge unit and the NRM on the AGICO JR-6A spinner magnetometer. Stepwise AF demagnetization was performed at successive peak fields of 0, 5, 10, 15, 20, and 30 mT up to a maximum of 60 mT. In addition, we performed stepwise thermal demagnetization up to a maximum temperature of 600°C on six sawed samples. The paleomagnetic intensities are weak, and inclinations are scattered between expected normal and reversed polarities. This makes it unclear if it was the primary magnetic signal or a pervasive overprint that was measured. Thermal demagnetization experiments show the presence of iron sulfides in the sediment.

The AMS results from Hole U1611A show an overall vertical direction of the κ_{min} axis with a scatter on the order of 10°, in agreement with observations of subhorizontal strata in the split cores.

6.4.4.4. Geochemistry

Headspace gas samples and IW in Hole U1611A were taken at one per recovered core or one every other half advance. Gas contents in both holes remained within a safe range, and the downhole pattern of methane/ethane ratios and absolute methane values are similar between the holes, despite a horizontal separation of 1361 m. IW salinities reached a maximum of 70 at ~1050 mbsf and then decreased below that depth. Major ion chemistry was used to interpret the origin of the saline IW to be a possible remnant of late Messinian brine. Partly because of this observation, we consulted with onshore microbiologists and took 5 cm whole-round samples (16 in total) from Hole U1611B at approximately 20 m intervals, directly adjacent and above the IW samples, using clean equipment and immediately froze them at −86°C for possible future microbiological analysis.

$CaCO_3$ varies from 5.0 to 92.0 wt% at Site U1611 with a mean of 28.3 wt%. $CaCO_3$ is generally between 30 and 60 wt% in the Pliocene Unit I during more Atlantic Ocean influenced conditions. In Unit II, carbonate decreases to between 14 and 36 wt%, and in Unit III it decreases further to the range of 15–25 wt%. In general, MSC sediments are dominated by clays and siliciclastics, with reduced carbonate production compared to the Pliocene. In Unit III, generally low carbonate concentrations are interrupted by decimeter-scale dolomitic or cemented carbonate beds with high values, typically greater than 60 wt% (seven samples).

In the uppermost ~865 m of Hole U1611A, TOC is generally <1 wt% and the C/N mean value is 13, indicating dominantly marine inputs. Below this interval is a sharp transition to higher TOC (up to 3 wt%) followed by generally decreasing TOC downcore from ~3 to 1 wt%, indicating decreasing productivity and/or preservation. C/N shifts at the same time as TOC to a mean of 19, indicating terrestrial inputs dominate, and farther downcore there is again a trend to a more mixed terrestrial and aquatic production. In this interval of generally elevated TOC, discrete horizons with organic fossils including fish, leaves, and wood also occur. One of several discrete black sedimentary layers was sampled and found to have a TOC of 52 wt%, consistent with an accumulation of biomass, with microscopic analysis suggesting immature organic matter. We suspect preservation is a primary control on the extraordinary organic matter at this site during the MSC associated with increasing stratification and anoxia of the water column and may signify the Alborán Basin's isolation from the Mediterranean Basin.

6.4.4.5. Physical properties and downhole measurements

Large-scale downhole patterns in the whole-round physical properties data from Holes U1611A and U1611B typically match well, but the same horizons are approximately 5–15 m shallower in Hole U1611B. Coarser lithologies tend to have lower NGR values. Cemented carbonate layers are distinguished by low NGR and MS values and relatively high GRA density values (Figure **F22**).

Downhole logging in Hole U1611A was only partially successful, with the triple combo tool string reaching 909 mbsf, logging a 236 m open hole interval. However, this interval includes the Messinian/Zanclean boundary at ~820 mbsf, providing stratigraphic continuity there, and also covers some poorly recovered Messinian intervals. The sonic-inclinometry tool string reached 743 mbsf before the hole became impassable. The borehole was characterized in the caliper borehole diameter log by washouts, bridges, and ledges. According to the General Purpose Inclinometry Tool (GPIT) logs, at the end of the pipe the borehole was inclined at ~9° from vertical and the inclination increased with depth to more than 12° at 750 mbsf.

7. Preliminary scientific assessment

7.1. Objective 1: to document the time at which the Atlantic first started to receive a distinct overflow from the Mediterranean and to evaluate quantitatively its role in Late Miocene global climate and regional environmental change

- Hypothesis 1.1: the earliest contourites formed as a result of Atlantic–Mediterranean exchange and correlate with the onset of Late Miocene SST decline in the mid- and high latitudes. Dating the first Atlantic–Mediterranean contourites will test this hypothesis.

Hypothesis 1.1 will require coring the fossil corridors in Spain and Morocco to test entirely. However, the records in the Atlantic also hold part of the story. The information collected that is relevant to this hypothesis is as follows:

- Site U1385: no contourites were recovered. This is consistent with its water depth, which is substantially below the core of the Mediterranean Overflow Water (MOW) plume today. However, the Miocene successions here, like the deeper water records cored during Expedition 397 at Sites U1586 and U1587 (Hodell et al., 2023), do record strong precessional cyclicity in NGR, and changes in the amplitude and thickness of these cycles do appear to correlate with the timing of major changes occurring in the Mediterranean during the MSC that have direct implications for Atlantic–Mediterranean exchange (Flecker et al., 2015).
- Site U1609: fine-grained silty mud contourites were recovered from the surface to 320 mbsf in Hole U1609A and 352 mbsf in Hole U1609B. The gradational nature of the transitions between subtle grain size differences make it difficult to be sure exactly where the onset is, and this will need to be resolved with detailed grain size analysis after the expedition. However, the identified onset corresponds broadly to the onset of the MSC in the Mediterranean (5.97 Ma). There is no evidence of contourites deeper in the succession.
- Site U1610: the uppermost 200 m recovered from Hole U1610A (500–700 mbsf) comprises silty mud contourites of Pliocene age (Figure **F6**). These beds are both siltier (e.g., coarser) and thicker than the equivalent-aged Early Pliocene contourites at Site U1609. This is consistent with their more proximal position relative to the Gibraltar Strait. At Site U1610, however, there is an interval between 700 and 935 mbsf that corresponds to the earliest Pliocene to latest Messinian (within the MSC; Figure **F6**), where no contourites were recovered, and there is no clear evidence of bottom water current activity of any sort. Again, this observation will need to be tested with high-resolution grain size analysis. Between 935 and 1030 mbsf, there are clear contourites. This interval is Messinian and is equivalent to the period just before and during the lower part of the MSC. More detailed correlation and dating will be required to ascertain exactly when these contouritic sediments start and end here. The succession from 1030 mbsf to the bottom of the hole (1400 mbsf) is dominated by sandstones deposited by turbidity

currents and mass flows. However, there is almost always evidence of reworking by bottom currents.

- Site U1611: the Pliocene succession recovered at this site in the Mediterranean is dominated by silty mud contourites. There is no evidence of contourite deposition below the Miocene/Pliocene boundary (Figure **F6**).

In summary, Site U1609 will be the best location for evaluating the timing of the initial onset of bottom water currents in the Tortonian when MO is thought to have started. It will also be necessary to establish that the bottom current features are not generated by other water masses. The contouritic information derived from the other sites is Messinian–Pliocene in age and provides interesting insights into bottom current variability through time.

- Hypothesis 1.2: atmospheric CO_2 sequestration in the deeper ocean through the initiation and development of Atlantic–Mediterranean Water (AMW) can account for the degree and distribution of SST cooling observed (reconstructing the velocity, density, and flux of AMW through time, quantifying its impact on CO_2 advection [Capella et al., 2019], and then modeling the resulting SST distribution [e.g., Ivanovic et al., 2014a] tests this hypothesis).
- Hypothesis 1.3: AMW modulates NADW formation, triggers glacial inception, and influences continental-scale aridification (model-based testing of this hypothesis requires the correlation of IMMAGE records with existing high-resolution records globally).

Testing Hypotheses 1.2 and 1.3 will require detailed postcruise analysis and modeling. However, a critical first step was to recover successions that could be tuned to the insolation curve as a means to achieving precessional-scale correlation between Expedition 401 sites and far-field locations of the same age. Given the depth our succession was buried, we anticipated 30%–40% core recovery, consistent with typical RCB recovery rates. However, not only was the recovery much better than this (>82% overall), but because our 8 Ma target was not buried as deeply as we had thought, there was time to drill not one but two holes at three of the four sites. At Site U1609, the two holes allowed us to generate a splice that is nearly complete (see Figure **F50** in the Site U1609 chapter [Flecker et al., 2025b]). We also have a close to complete record at Site U1385 (see Figure **F50** in the Site U1385 chapter [Flecker et al., 2025a]) that can be correlated peak-to-peak to the adjacent orbitally tuned NGR records from Sites U1586 and U1587 (Hodell et al., 2023). Finally, although the recovery of the single hole at Site U1610 was only 80%, most of the poor recovery is toward the bottom of the hole. The upper part of the succession is strongly cyclic, making it likely that it will be possible to tune the record to the insolation curve.

Taken together, the cores recovered during Expedition 401 place us in a far better position to test these hypotheses than could ever have been anticipated before the expedition.

7.2. Objective 2: to recover a complete record of Atlantic–Mediterranean exchange before, during, and after the Messinian Salinity Crisis and to evaluate the causes and consequences of this extreme oceanographic event locally, regionally, and globally

- Hypothesis 2.1: the Alborán Basin was an intermediate marine system influenced by the Atlantic and separated from the Mediterranean by the Alborán volcanic arc during the MSC.

Cores recovered at Site U1611 in the Alborán Sea record a thick succession of organic-rich, laminated, fine-grained sediments interbedded with turbidites, debrites, and slumps that is overlain by Pliocene contourites. The fauna and ichnofossils identified in the pre-Pliocene sequence indicate that subaqueous deposition occurred throughout in a water mass that was highly stratified with low oxygen or anoxic conditions at the sediment/water interface. The bottom of the hole is younger than 6.82 Ma, and fine-grained, laminated, low-oxygen sediment dominate the sequence from the base to the Miocene/Pliocene boundary. Although the onset of the MSC has been identified on the basis of faunal changes (lower diversity and smaller sizes), the sequence recovered at Site U1611 does not resemble the typical Mediterranean succession, which mainly comprises evaporites and sediments barren of fauna (e.g., Krijgsman et al., 2024). Instead, at Site U1611 the sequence contains no evaporites and very few completely barren horizons. In this respect, the Alborán Sea appears to resemble the Atlantic more than the Mediterranean, although the laminated sediments are clearly different from the well-bioturbated successions that characterize open ocean settings. On balance, then it is likely that the Alborán Sea was an intermediate marine system during the MSC, although the details of its connectivity with the Atlantic and Mediterranean remain unclear at this stage. We drilled two holes at this site, and Hole U1611B in particular is largely complete (78%) because of the drilling configuration we employed (half-advance coring using the RCB coring system and a PDC bit). The majority of what was not recovered was in the Pliocene, so the record from the Miocene–Pliocene downward (with the exception of a 2 m gap just below the Miocene/Pliocene boundary) is close to continuous. This will make testing Hypothesis 2.1 in detail possible with additional postcruise analysis.

- Hypothesis 2.2: extreme environmental fluctuations in the Mediterranean had negligible impact on AMW.

Hypothesis 2.2 requires the tuning of both Mediterranean and Atlantic records to the insolation curve to compare the timing of changes in the physical properties reflecting Late Miocene water mass and sedimentation changes. Although the details of this tuning require refinement, substantial changes in the Atlantic physical properties records occur at times consistent with major changes in the Mediterranean associated with gateway changes. Exploration of the mechanisms for achieving these synchronous changes can now be implemented through postcruise empirical and modeling studies.

7.3. Objective 3: to test our quantitative understanding of the behavior of ocean overflow plumes during the most extreme exchange in Earth's history

- Hypothesis 3.1: the velocity of the plume is a function of the Atlantic–Mediterranean density contrast, limitation on flow through the strait (Bryden et al., 1994), the gradient of the slope, and the degree of mixing (Price et al., 1993).
- Hypothesis 3.2: mixing with ambient water causes a strong negative feedback on the size of the plume, limiting the degree of its variability (Price et al., 1993). This means that only minor changes in the physical size of the plume are expected, despite the proportion of plume water derived directly from the outflow varying significantly. As a result, changes in Mediterranean density have little impact on the plume position.
- Hypothesis 3.3: the main control on the settling depth of MO is the vertical density gradient in the North Atlantic, which is a product of North Atlantic overturning circulation (Rogerson et al., 2012a).

Testing these physical oceanography hypotheses will require detailed physical and chemical analysis and modeling. However, this is only possible because of the high recovery rates with clear and tunable cyclicity enabling site-to-site correlation down the MO plume on a precessional timescale. The cores we have recovered will permit us to test whether the representations of overflows within general circulation models are effective when overflow density is higher than the range of validation provided by the modern ocean. If general circulation model representation of these Messinian high density overflows are inadequate, this casts doubt on all modeling experiments in which part of the ocean-atmosphere system is outside the range exhibited today.

References

Abrantes, F., 2000. 200,000 yr diatom records from Atlantic upwelling sites reveal maximum productivity during LGM and a shift in phytoplankton community structure at 185 000 yr. Earth and Planetary Science Letters, 176(1):7–16. **https://doi.org/10.1016/S0012-821X(99)00312-X**

Alhammoud, B., Meijer, P.T., and Dijkstra, H.A., 2010. Sensitivity of Mediterranean thermohaline circulation to gateway depth: a model investigation. Paleoceanography, 25(2):PA2220. **https://doi.org/10.1029/2009PA001823**

Álvarez, M., Pérez, F.F., Shoosmith, D.R., and Bryden, H.L., 2005. Unaccounted role of Mediterranean water in the drawdown of anthropogenic carbon. Journal of Geophysical Research: Oceans, 110(C9):C09S03. **https://doi.org/10.1029/2004JC002633**

Ambar, I., Serra, N., Brogueira, M.J., Cabeçadas, G., Abrantes, F., Freitas, P., Gonçalves, C., and Gonzalez, N., 2002. Physical, chemical and sedimentological aspects of the Mediterranean outflow off Iberia. Deep Sea Research, Part II: Topical Studies in Oceanography, 49(19):4163–4177. **https://doi.org/10.1016/S0967-0645(02)00148-0**
Bahr, A., Kaboth, S., Jiménez-Espejo, F.J., Sierro, F.J., Voelker, A.H.L., Lourens, L., Röhl, U., Reichart, G.J., Escutia, C., Hernández-Molina, F.J., Pross, J., and Friedrich, O., 2015. Persistent monsoonal forcing of Mediterranean Outflow Water dynamics during the late Pleistocene. Geology, 43(11):951–954. **https://doi.org/10.1130/G37013.1**
Bahr, A., Kaboth-Bahr, S., and Karas, C., 2022. The opening and closure of oceanic seaways during the Cenozoic: pacemaker of global climate change? Special Publication - Geological Society of London, 523:SP523-2021-2054. **https://doi.org/10.1144/SP523-2021-54**
Benson, R.H., Rakic-El Bied, K., and Bonaduce, G., 1991. An important current reversal (influx) in the Rifian Corridor (Morocco) at the Tortonian-Messinian boundary: the end of Tethys Ocean. Paleoceanography, 6(1):165–192. **https://doi.org/10.1029/90PA00756**
Bigg, G.R., Jickells, T.D., Liss, P.S., and Osborn, T.J., 2003. The role of the oceans in climate. International Journal of Climatology, 23(10):1127–1159. **https://doi.org/10.1002/joc.926**
Bigg, G.R., and Wadley, M.R., 2001. Millennial-scale variability in the oceans: an ocean modelling view. Journal of Quaternary Science, 16(4):309–319. **https://doi.org/10.1002/jqs.599**
Billups, K., 2002. Late Miocene through early Pliocene deep water circulation and climate change viewed from the sub-Antarctic South Atlantic. Palaeogeography, Palaeoclimatology, Palaeoecology, 185(3–4):287–307. **https://doi.org/10.1016/S0031-0182(02)00340-1**
Blanc, P.-L., 2006. Improved modelling of the Messinian salinity crisis and conceptual implications. Palaeogeography, Palaeoclimatology, Palaeoecology, 238(1):349–372. **https://doi.org/10.1016/j.palaeo.2006.03.033**
Booth-Rea, G., R. Ranero, C., and Grevemeyer, I., 2018. The Alboran volcanic-arc modulated the Messinian faunal exchange and salinity crisis. Scientific Reports, 8(1):13015. **https://doi.org/10.1038/s41598-018-31307-7**
Broecker, W.S., 1991. The great ocean conveyor. Oceanography, 4(2):79–89. **http://www.jstor.org/stable/43924572**
Bryden, H.L., Candela, J., and Kinder, T.H., 1994. Exchange through the Strait of Gibraltar. Progress in Oceanography, 33(3):201–248. **https://doi.org/10.1016/0079-6611(94)90028-0**
Bulian, F., Sierro, F.J., Ledesma, S., Jiménez-Espejo, F.J., and Bassetti, M.-A., 2021. Messinian West Alboran Sea record in the proximity of Gibraltar: Early signs of Atlantic-Mediterranean gateway restriction. Marine Geology, 434:106430. **https://doi.org/10.1016/j.margeo.2021.106430**
Capella, W., Flecker, R., Hernández-Molina, F.J., Simon, D., Meijer, P.T., Rogerson, M., Sierro, F.J., and Krijgsman, W., 2019. Mediterranean isolation preconditioning the Earth System for Late Miocene climate cooling. Scientific Reports, 9(1):3795. **https://doi.org/10.1038/s41598-019-40208-2**
Capella, W., Hernández-Molina, F.J., Flecker, R., Hilgen, F.J., Hssain, M., Kouwenhoven, T.J., van Oorschot, M., Sierro, F.J., Stow, D.A.V., Trabucho-Alexandre, J., Tulbure, M.A., de Weger, W., Yousfi, M.Z., and Krijgsman, W., 2017. Sandy contourite drift in the late Miocene Rifian Corridor (Morocco): Reconstruction of depositional environments in a foreland-basin seaway. Sedimentary Geology, 355:31-57. **https://doi.org/10.1016/j.sedgeo.2017.04.004**
de Weger, W., Hernández-Molina, F.J., Flecker, R., Sierro, F.J., Chiarella, D., Krijgsman, W., and Manar, M.A., 2020. Late Miocene contourite channel system reveals intermittent overflow behavior. Geology, 48(12):1194–1199. **https://doi.org/10.1130/G47944.1**
de Weger, W., Hernández-Molina, F.J., Miguez-Salas, O., de Castro, S., Bruno, M., Chiarella, D., Sierro, F.J., Blackbourn, G., and Manar, M.A., 2021. Contourite depositional system after the exit of a strait: case study from the late Miocene South Rifian Corridor, Morocco. Sedimentology, 68(7):2996–3032. **https://doi.org/10.1111/sed.12882**
Dietrich, D.E., Tseng, Y.-H., Medina, R., Piacsek, S.A., Liste, M., Olabarrieta, M., Bowman, M.J., and Mehra, A., 2008. Mediterranean Overflow Water (MOW) simulation using a coupled multiple-grid Mediterranean Sea/North Atlantic Ocean model. Journal of Geophysical Research: Oceans, 113(C7):C07027. **https://doi.org/10.1029/2006JC003914**
Dixon, R.K., Solomon, A.M., Brown, S., Houghton, R.A., Trexier, M.C., and Wisniewski, J., 1994. Carbon pools and flux of global forest ecosystems. Science, 263(5144):185–190. **https://doi.org/10.1126/science.263.5144.185**
Do Couto, D., Gorini, C., Jolivet, L., Lebret, N., Augier, R., Gumiaux, C., d'Acremont, E., Ammar, A., Jabour, H., and Auxietre, J.-L., 2016. Tectonic and stratigraphic evolution of the Western Alboran Sea Basin in the last 25 Myrs. Tectonophysics, 677–678:280–311. **https://doi.org/10.1016/j.tecto.2016.03.020**
Duggen, S., Hoernle, K., van den Bogaard, P., Rüpke, L., and Phipps Morgan, J., 2003. Deep roots of the Messinian salinity crisis. Nature, 422(6932):602–606. **https://doi.org/10.1038/nature01553**
Elsworth, G., Galbraith, E., Halverson, G., and Yang, S., 2017. Enhanced weathering and CO_2 drawdown caused by latest Eocene strengthening of the Atlantic meridional overturning circulation. Nature Geoscience, 10(3):213–216. **https://doi.org/10.1038/ngeo2888**
Ercilla, G., Juan, C., Hernández-Molina, F.J., Bruno, M., Estrada, F., Alonso, B., Casas, D., Farran, M.l., Llave, E., García, M., Vázquez, J.T., D'Acremont, E., Gorini, C., Palomino, D., Valencia, J., El Moumni, B., and Ammar, A., 2016. Significance of bottom currents in deep-sea morphodynamics: an example from the Alboran Sea. Marine Geology, 378:157–170. **https://doi.org/10.1016/j.margeo.2015.09.007**
Estrada, F., Ercilla, G., Gorini, C., Alonso, B., Vázquez, J.T., García-Castellanos, D., Juan, C., Maldonado, A., Ammar, A., and Elabbassi, M., 2011. Impact of pulsed Atlantic water inflow into the Alboran Basin at the time of the Zanclean flooding. Geo-Marine Letters, 31(5):361–376. **https://doi.org/10.1007/s00367-011-0249-8**
Expedition 339 Scientists, 2013. Expedition 339 summary. In Stow, D.A.V., Hernández-Molina, F.J., Alvarez Zarikian, C.A., and the Expedition 339 Scientists, Proceedings of the Integrated Ocean Drilling Program. 339: Tokyo (Integrated Ocean Drilling Program Management International, Inc.). **https://doi.org/10.2204/iodp.proc.339.101.2013**

Faccenna, C., Piromallo, C., Crespo-Blanc, A., Jolivet, L., and Rossetti, F., 2004. Lateral slab deformation and the origin of the western Mediterranean arcs. Tectonics, 23(1):TC1012. **https://doi.org/10.1029/2002TC001488**

Flecker, R., Ducassou, E., and Williams, T., 2023. Expedition 401 Scientific Prospectus: Mediterranean Atlantic Gateway Exchange. International Ocean Discovery Program. **https://doi.org/10.14379/iodp.sp.401.2023**

Flecker, R., Ducassou, E., Williams, T., Amarathunga, U., Balestra, B., Berke, M.A., Blättler, C.L., Chin, S., Das, M., Egawa, K., Fabregas, N., Feakins, S.J., George, S.C., Hernández-Molina, F.J., Krijgsman, W., Li, Z., Liu, J., Noto, D., Raad, F., Rodríguez-Tovar, F.J., Sierro, F.J., Standring, P., Stine, J., Tanaka, E., Teixeira, M., Xu, X., Yin, S., and Yousfi, M.Z., 2025a. Site U1385. In Flecker, R., Ducassou, E., Williams, T., and the Expedition 401 Scientists, Mediterranean–Atlantic Gateway Exchange. Proceedings of the International Ocean Discovery Program, 401: College Station, TX (International Ocean Discovery Program). **https://doi.org/10.14379/iodp.proc.401.105.2025**

Flecker, R., Ducassou, E., Williams, T., Amarathunga, U., Balestra, B., Berke, M.A., Blättler, C.L., Chin, S., Das, M., Egawa, K., Fabregas, N., Feakins, S.J., George, S.C., Hernández-Molina, F.J., Krijgsman, W., Li, Z., Liu, J., Noto, D., Raad, F., Rodríguez-Tovar, F.J., Sierro, F.J., Standring, P., Stine, J., Tanaka, E., Teixeira, M., Xu, X., Yin, S., and Yousfi, M.Z., 2025b. Site U1609. In Flecker, R., Ducassou, E., Williams, T., and the Expedition 401 Scientists, Mediterranean–Atlantic Gateway Exchange. Proceedings of the International Ocean Discovery Program, 401: College Station, TX (International Ocean Discovery Program). **https://doi.org/10.14379/iodp.proc.401.103.2025**

Flecker, R., Ducassou, E., Williams, T., Amarathunga, U., Balestra, B., Berke, M.A., Blättler, C.L., Chin, S., Das, M., Egawa, K., Fabregas, N., Feakins, S.J., George, S.C., Hernández-Molina, F.J., Krijgsman, W., Li, Z., Liu, J., Noto, D., Raad, F., Rodríguez-Tovar, F.J., Sierro, F.J., Standring, P., Stine, J., Tanaka, E., Teixeira, M., Xu, X., Yin, S., and Yousfi, M.Z., 2025c. Site U1610. In Flecker, R., Ducassou, E., Williams, T., and the Expedition 401 Scientists, Mediterranean–Atlantic Gateway Exchange. Proceedings of the International Ocean Discovery Program, 401: College Station, TX (International Ocean Discovery Program). **https://doi.org/10.14379/iodp.proc.401.104.2025**

Flecker, R., Ducassou, E., Williams, T., Amarathunga, U., Balestra, B., Berke, M.A., Blättler, C.L., Chin, S., Das, M., Egawa, K., Fabregas, N., Feakins, S.J., George, S.C., Hernández-Molina, F.J., Krijgsman, W., Li, Z., Liu, J., Noto, D., Raad, F., Rodríguez-Tovar, F.J., Sierro, F.J., Standring, P., Stine, J., Tanaka, E., Teixeira, M., Xu, X., Yin, S., and Yousfi, M.Z., 2025d. Site U1611. In Flecker, R., Ducassou, E., Williams, T., and the Expedition 401 Scientists, Mediterranean–Atlantic Gateway Exchange. Proceedings of the International Ocean Discovery Program, 401: College Station, TX (International Ocean Discovery Program). **https://doi.org/10.14379/iodp.proc.401.106.2025**

Flecker, R., Krijgsman, W., Capella, W., de Castro Martíns, C., Dmitrieva, E., Mayser, J.P., Marzocchi, A., Modestou, S., Ochoa, D., Simon, D., Tulbure, M., van den Berg, B., van der Schee, M., de Lange, G., Ellam, R., Govers, R., Gutjahr, M., Hilgen, F., Kouwenhoven, T., Lofi, J., Meijer, P., Sierro, F.J., Bachiri, N., Barhoun, N., Alami, A.C., Chacon, B., Flores, J.A., Gregory, J., Howard, J., Lunt, D., Ochoa, M., Pancost, R., Vincent, S., and Yousfi, M.Z., 2015. Evolution of the Late Miocene Mediterranean–Atlantic gateways and their impact on regional and global environmental change. Earth-Science Reviews, 150:365–392. **https://doi.org/10.1016/j.earscirev.2015.08.007**

Garcia-Castellanos, D., Micallef, A., Estrada, F., Camerlenghi, A., Ercilla, G., Periáñez, R., and Abril, J.M., 2020. The Zanclean megaflood of the Mediterranean – searching for independent evidence. Earth-Science Reviews, 201:103061. **https://doi.org/10.1016/j.earscirev.2019.103061**

García-Gallardo, Á., Grunert, P., Van der Schee, M., Sierro, F.J., Jiménez-Espejo, F.J., Alvarez Zarikian, C.A., and Piller, W.E., 2017a. Benthic foraminifera-based reconstruction of the first Mediterranean-Atlantic exchange in the early Pliocene Gulf of Cadiz. Palaeogeography, Palaeoclimatology, Palaeoecology, 472:93–107. **https://doi.org/10.1016/j.palaeo.2017.02.009**

García-Gallardo, Á., Grunert, P., Voelker, A.H.L., Mendes, I., and Piller, W.E., 2017b. Re-evaluation of the "elevated epifauna" as indicator of Mediterranean outflow water in the Gulf of Cadiz using stable isotopes ($\delta^{13}C$, $\delta^{18}O$). Global and Planetary Change, 155:78–97. **https://doi.org/10.1016/j.gloplacha.2017.06.005**

Glazkova, T., Hernández-Molina, F.J., Dorokhova, E., Mena, A., Roque, C., Rodríguez-Tovar, F.J., Krechik, V., Kuleshova, L., and Llave, E., 2022. Sedimentary processes in the Discovery Gap (Central–NE Atlantic): An example of a deep marine gateway. Deep Sea Research Part I: Oceanographic Research Papers, 180:103681. **https://doi.org/10.1016/j.dsr.2021.103681**

Grant, K.M., Rohling, E.J., Westerhold, T., Zabel, M., Heslop, D., Konijnendijk, T., and Lourens, L., 2017. A 3 million year index for North African humidity/aridity and the implication of potential pan-African Humid periods. Quaternary Science Reviews, 171:100–118. **https://doi.org/10.1016/j.quascirev.2017.07.005**

Guerra-Merchán, A., Serrano, F., Garcés, M., Gofas, S., Esu, D., Gliozzi, E., and Grossi, F., 2010. Messinian Lago-Mare deposits near the Strait of Gibraltar (Malaga Basin, S Spain). Palaeogeography, Palaeoclimatology, Palaeoecology, 285(3):264–276. **https://doi.org/10.1016/j.palaeo.2009.11.019**

Hernández-Molina, F.J., Larter, R.D., and Maldonado, A., 2017. Neogene to Quaternary stratigraphic evolution of the Antarctic Peninsula, Pacific Margin offshore of Adelaide Island: Transitions from a non-glacial, through glacially-influenced to a fully glacial state. Global and Planetary Change, 156:80–111. **https://doi.org/10.1016/j.gloplacha.2017.07.002**

Hernández-Molina, F.J., Llave, E., Preu, B., Ercilla, G., Fontan, A., Bruno, M., Serra, N., Gomiz, J.J., Brackenridge, R.E., Sierro, F.J., Stow, D.A.V., García, M., Juan, C., Sandoval, N., and Arnaiz, A., 2014a. Contourite processes associated with the Mediterranean Outflow Water after its exit from the Strait of Gibraltar: global and conceptual implications. Geology, 42(3):227–230. **https://doi.org/10.1130/G35083.1**

Hernández-Molina, F.J., Serra, N., Stow, D.A.V., Llave, E., Ercilla, G., and Van Rooij, D., 2011. Along-slope oceanographic processes and sedimentary products around the Iberian margin. Geo-Marine Letters, 31(5):315–341. **https://doi.org/10.1007/s00367-011-0242-2**

Hernández-Molina, F.J., Sierro, F.J., Llave, E., Roque, C., Stow, D.A.V., Williams, T., Lofi, J., Van der Schee, M., Arnáiz, A., Ledesma, S., Rosales, C., Rodríguez-Tovar, F.J., Pardo-Igúzquiza, E., and Brackenridge, R.E., 2016. Evolution of the Gulf of Cadiz margin and southwest Portugal contourite depositional system: tectonic, sedimentary and paleoceanographic implications from IODP Expedition 339. Marine Geology, 377:7–39. **https://doi.org/10.1016/j.margeo.2015.09.013**

Hernández-Molina, F.J., Stow, D.A.V., Alvarez-Zarikian, C.A., Acton, G., Bahr, A., Balestra, B., Ducassou, E., Flood, R., Flores, J.-A., Furota, S., Grunert, P., Hodell, D., Jimenez-Espejo, F., Kim, J.K., Krissek, L., Kuroda, J., Li, B., Llave, E., Lofi, J., Lourens, L., Miller, M., Nanayama, F., Nishida, N., Richter, C., Roque, C., Pereira, H., Sanchez Goñi, M.F., Sierro, F.J., Singh, A.D., Sloss, C., Takashimizu, Y., Tzanova, A., Voelker, A., Williams, T., and Xuan, C., 2014b. Onset of Mediterranean outflow into the North Atlantic. Science, 344(6189):1244–1250. **https://doi.org/10.1126/science.1251306**

Hernández-Molina, J., Llave, E., Somoza, L., Fernández-Puga, M.C., Maestro, A., León, R., Medialdea, T., Barnolas, A., García, M., Díaz del Río, V., Fernández-Salas, L.M., Vázquez, J.T., Lobo, F., Alveirinho Dias, J.M., Rodero, J., and Gardner, J., 2003. Looking for clues to paleoceanographic imprints: a diagnosis of the Gulf of Cadiz contourite depositional systems. Geology, 31(1):19–22. **https://doi.org/10.1130/0091-7613(2003)031%3C0019:LFCTPI%3E2.0.CO;2**

Hilgen, F., Aziz, H.A., Bice, D., Iaccarino, S., Krijgsman, W., Kuiper, K., Montanari, A., Raffi, I., Turco, E., and Zachariasse, W.-J., 2005. The global boundary stratotype section and point (GSSP) of the Tortonian Stage (Upper Miocene) at Monte Dei Corvi. International Union of Geological Sciences, 28(1):6–17. **https://doi.org/10.18814/epiiugs/2005/v28i1/001**

Hodell, D., Lourens, L., Crowhurst, S., Konijnendijk, T., Tjallingii, R., Jiménez-Espejo, F., Skinner, L., Tzedakis, P.C., and the Shackleton Site Project Members, 2015. A reference time scale for Site U1385 (Shackleton Site) on the SW Iberian Margin. Global and Planetary Change, 133:49–64. **https://doi.org/10.1016/j.gloplacha.2015.07.002**

Hodell, D.A., Abrantes, F., Alvarez Zarikian, C.A., and the Expedition 397 Scientists, 2023. Expedition 397 Preliminary Report: Iberian Margin Paleoclimate. International Ocean Discovery Program. **https://doi.org/10.14379/iodp.pr.397.2023**

Hsü, K.J., Ryan, W.B.F., and Cita, M.B., 1973. Late Miocene desiccation of the Mediterranean. Nature, 242(5395):240–244. **https://doi.org/10.1038/242240a0**

Iaccarino, S.M., and Bossio, A., 1999. Paleoenvironment of uppermost Messinian sequences in the western Mediterranean (Sites 974, 975, and 978). In Zahn, R., Comas, M.C., and Klaus, A. (Eds.), Proceedings of the Ocean Drilling Program, Scientific Results. 161: College Station, TX (Ocean Drilling Program). **https://doi.org/10.2973/odp.proc.sr.161.246.1999**

Intergovernmental Panel on Climate Change, 2014. Climate Change 2013 – The Physical Science Basis: Cambridge, UK (Cambridge University Press). **https://doi.org/10.1017/CBO9781107415324.013**

Iorga, M.C., and Lozier, M.S., 1999. Signatures of the Mediterranean outflow from a North Atlantic climatology: 1. Salinity and density fields. Journal of Geophysical Research: Oceans, 104(C11):25985–26009. **https://doi.org/10.1029/1999JC900115**

Ivanovic, R.F., Valdes, P.J., Flecker, R., Gregoire, L.J., and Gutjahr, M., 2013. The parameterisation of Mediterranean–Atlantic water exchange in the Hadley Centre model HadCM3, and its effect on modelled North Atlantic climate. Ocean Modelling, 62:11–16. **https://doi.org/10.1016/j.ocemod.2012.11.002**

Ivanovic, R.F., Valdes, P.J., Flecker, R., and Gutjahr, M., 2014a. Modelling global-scale climate impacts of the late Miocene Messinian salinity crisis. Climate of the Past, 10(2):607–622. **https://doi.org/10.5194/cp-10-607-2014**

Ivanovic, R.F., Valdes, P.J., Gregoire, L., Flecker, R., and Gutjahr, M., 2014b. Sensitivity of modern climate to the presence, strength and salinity of Mediterranean-Atlantic exchange in a global general circulation model. Climate Dynamics, 42(3):859–877. **https://doi.org/10.1007/s00382-013-1680-5**

Jolivet, L., and Faccenna, C., 2000. Mediterranean extension and the Africa-Eurasia collision. Tectonics, 19(6):1095–1106. **https://doi.org/10.1029/2000TC900018**

Juan, C., Ercilla, G., Estrada, F., Alonso, B., Casas, D., Vázquez, J.T., d'Acremont, E., Medialdea, T., Hernández-Molina, F.J., Gorini, C., El Moumni, B., and Valencia, J., 2020. Multiple factors controlling the deep marine sedimentation of the Alboran Sea (SW Mediterranean) after the Zanclean Atlantic mega-flood. Marine Geology, 423:106138. **https://doi.org/10.1016/j.margeo.2020.106138**

Juan, C., Ercilla, G., Hernández-Molina, F.J., Estrada, F., Alonso, B., Casas, D., García, M., Farran, M.l., Llave, E., Palomino, D., Vázquez, J.-T., Medialdea, T., Gorini, C., D'Acremont, E., El Moumni, B., and Ammar, A., 2016. Seismic evidence of current-controlled sedimentation in the Alboran Sea during the Pliocene and Quaternary: palaeoceanographic implications. Marine Geology, 378:292–311. **https://doi.org/10.1016/j.margeo.2016.01.006**

Kaboth-Bahr, S., Bahr, A., Zeeden, C., Toucanne, S., Eynaud, F., Jiménez-Espejo, F., Röhl, U., Friedrich, O., Pross, J., Löwemark, L., and Lourens, L.J., 2018. Monsoonal forcing of European ice-sheet dynamics during the late Quaternary. Geophysical Research Letters, 45(14):7066–7074. **https://doi.org/10.1029/2018GL078751**

Kaminski, M.A., Aksu, A., Box, M., Hiscott, R.N., Filipescu, S., and Al-Salameen, M., 2002. Late Glacial to Holocene benthic foraminifera in the Marmara Sea: implications for Black Sea–Mediterranean Sea connections following the last deglaciation. Marine Geology, 190(1):165–202. **https://doi.org/10.1016/S0025-3227(02)00347-X**

Karas, C., Nürnberg, D., Bahr, A., Groeneveld, J., Herrle, J.O., Tiedemann, R., and deMenocal, P.B., 2017. Pliocene oceanic seaways and global climate. Scientific Reports, 7(1):39842. **https://doi.org/10.1038/srep39842**

Kennett, J.P., 1982. Marine Geology: Englewood Cliffs, NJ (Prentice-Hall).

Khélifi, N., Sarnthein, M., Andersen, N., Blanz, T., Frank, M., Garbe-Schönberg, D., Haley, B.A., Stumpf, R., and Weinelt, M., 2009. A major and long-term Pliocene intensification of the Mediterranean outflow, 3.5–3.3 Ma ago. Geology, 37(9):811–814. **https://doi.org/10.1130/G30058A.1**

Knutz, P.C., 2008. Palaeoceanographic significance of contourite drifts. In Rebesco, M., and Camerlenghi, A. (Eds.), Contourites. Developments in Sedimentology, 60: (Elsevier), 511–535. **https://doi.org/10.1016/S0070-4571(08)10024-3**

Krijgsman, W., Capella, W., Simon, D., Hilgen, F.J., Kouwenhoven, T.J., Meijer, P.T., Sierro, F.J., Tulbure, M.A., van den Berg, B.C.J., van der Schee, M., and Flecker, R., 2018. The Gibraltar Corridor: Watergate of the Messinian Salinity Crisis. Marine Geology, 403:238–246. **https://doi.org/10.1016/j.margeo.2018.06.008**

Krijgsman, W., Rohling, E.J., Palcu, D.V., Raad, F., Amarathunga, U., Flecker, R., Florindo, F., Roberts, A.P., Sierro, F.J., and Aloisi, G., 2024. Causes and consequences of the Messinian salinity crisis. Nature Reviews Earth & Environment, 5(5):335–350. **https://doi.org/10.1038/s43017-024-00533-1**

LaRiviere, J.P., Ravelo, A.C., Crimmins, A., Dekens, P.S., Ford, H.L., Lyle, M., and Wara, M.W., 2012. Late Miocene decoupling of oceanic warmth and atmospheric carbon dioxide forcing. Nature, 486(7401):97–100. **https://doi.org/10.1038/nature11200**

Ledesma, S., 2000. Astrobiocronología y Estratigrafía de Alta Resolución del Neógeno de la Cuenca del Guadalquivir-Golfo de Cadiz [PhD dissertation]. University of Salamanca, Salamanca, Spain.

Legg, S., Briegleb, B., Chang, Y., Chassignet, E.P., Danabasoglu, G., Ezer, T., Gordon, A.L., Griffies, S., Hallberg, R., Jackson, L., Large, W., Özgökmen, T.M., Peters, H., Price, J., Riemenschneider, U., Wu, W., Xu, X., and Yang, J., 2009. Improving oceanic overflow representation in climate models: the gravity current entrainment climate process team. Bulletin of the American Meteorological Society, 90(5):657–670. **https://doi.org/10.1175/2008BAMS2667.1**

Llave, E., Hernández-Molina, F.J., García, M., Ercilla, G., Roque, C., Juan, C., Mena, A., Preu, B., Rooij, D.V., Rebesco, M., Brackenridge, R., Jané, G., Gómez-Ballesteros, M., and Stow, D., 2020. Contourites along the Iberian continental margins: conceptual and economic implications. Geological Society, London, Special Publications, 476(1):403–436. **https://doi.org/10.1144/SP476-2017-46**

Llave, E., Matias, H., Hernández-Molina, F.J., Ercilla, G., Stow, D.A.V., and Medialdea, T., 2011. Pliocene–Quaternary contourites along the northern Gulf of Cadiz margin: sedimentary stacking pattern and regional distribution. Geo-Marine Letters, 31(5):377–390. **https://doi.org/10.1007/s00367-011-0241-3**

Lofi, J., 2018. Seismic Atlas of the Messinian Salinity Crisis Markers in the Mediterranean Sea, Volume 2: Paris (Société géologique de France).

Magill, C.R., Ausín, B., Wenk, P., McIntyre, C., Skinner, L., Martínez-García, A., Hodell, D.A., Haug, G.H., Kenney, W., and Eglinton, T.I., 2018. Transient hydrodynamic effects influence organic carbon signatures in marine sediments. Nature Communications, 9(1):4690. **https://doi.org/10.1038/s41467-018-06973-w**

Maldonado, A., Somoza, L.s., and Pallarés, L., 1999. The Betic orogen and the Iberian–African boundary in the Gulf of Cadiz: geological evolution (central North Atlantic). Marine Geology, 155(1):9–43. **https://doi.org/10.1016/S0025-3227(98)00139-X**

Martín, J.M., Braga, J.C., Aguirre, J., and Puga-Bernabéu, Á., 2009. History and evolution of the North-Betic Strait (Prebetic Zone, Betic Cordillera): a narrow, early Tortonian, tidal-dominated, Atlantic–Mediterranean marine passage. Sedimentary Geology, 216(3):80–90. **https://doi.org/10.1016/j.sedgeo.2009.01.005**

Martín, J.M., Puga-Bernabéu, Á., Aguirre, J., and Braga, J.C., 2014. Miocene Atlantic-Mediterranean seaways in the Betic Cordillera (southern Spain). Revista de la Sociedad Geológica de España, 27(1):175–186.

Martínez del Olmo, W., 2011. El Messiniense en el Golfo de Valencia y el Mar de Alborán: implicaciones paleogeográficas y paleoceanográficas. Revista de la Sociedad Geológica de España, 24(3-4):237–257.

Martínez del Olmo, W., and Comas, M.C., 2008. Arquitectura sísmica, olistostromas y fallas extensionales en el norte de la cuenca oeste del Mar de Alborán. Revista de la Sociedad Geológica de España, 21(3–4):151–167. **https://dialnet.unirioja.es/servlet/articulo?codigo=3112411**

Martínez del Olmo, W., and Martín, D., 2016. El Neógeno de la cuenca Guadalquivir-Cádiz (Sur de España). Revista de la Sociedad Geológica de España, 29(1):35–58.

Marzocchi, A., Lunt, D.J., Flecker, R., Bradshaw, C.D., Farnsworth, A., and Hilgen, F.J., 2015. Orbital control on Late Miocene climate and the North African monsoon: insight from an ensemble of sub-precessional simulations. Climate of the Past, 11(10):1271–1295. **https://doi.org/10.5194/cp-11-1271-2015**

Nelson, C.H., Baraza, J., Maldonado, A., Rodero, J., Escutia, C., and Barber Jr, J.H., 1999. Influence of the Atlantic inflow and Mediterranean outflow currents on late Quaternary sedimentary facies of the Gulf of Cadiz continental margin. Marine Geology, 155(1–2):99–129. **https://doi.org/10.1016/S0025-3227(98)00143-1**

Ng, Z.L., Hernández-Molina, F.J., Ledesma, S., Sierro, F.J., Duarte, D., Llave, E., Roque, C., and Arnáiz, Á., 2022. Late Miocene evolution of the eastern Deep Algarve basin: interaction of bottom currents and gravitational processes in a foredeep setting. Marine and Petroleum Geology, 141:105695. **https://doi.org/10.1016/j.marpetgeo.2022.105695**

Nisancioglu, K.H., Raymo, M.E., and Stone, P.H., 2003. Reorganization of Miocene deep water circulation in response to the shoaling of the Central American Seaway. Paleoceanography, 18(1):1006–1018. **https://doi.org/10.1029/2002PA000767**

Orszag-Sperber, F., 2006. Changing perspectives in the concept of "Lago-Mare" in Mediterranean Late Miocene evolution. Sedimentary Geology, 188–189:259–277. **https://doi.org/10.1016/j.sedgeo.2006.03.008**

Peixoto, J.P., and Kettani, M.A., 1973. The control of the water cycle. Scientific American, 228(4):46–63. **http://www.jstor.org/stable/24923025**

Penaud, A., Eynaud, F., Sánchez-Goñi, M., Malaizé, B., Turon, J.L., and Rossignol, L., 2011. Contrasting sea-surface responses between the western Mediterranean Sea and eastern subtropical latitudes of the North Atlantic during abrupt climatic events of MIS 3. Marine Micropaleontology, 80(1):1–17. **https://doi.org/10.1016/j.marmicro.2011.03.002**

Price, J.F., Baringer, M.O.N., Lueck, R.G., Johnson, G.C., Ambar, I., Parrilla, G., Cantos, A., Kennelly, M.A., and Sanford, T.B., 1993. Mediterranean Outflow mixing and dynamics. Science, 259(5099):1277–1282. **https://doi.org/10.1126/science.259.5099.1277**

Price, J.F., and O'Neil Baringer, M., 1994. Outflows and deep water production by marginal seas. Progress in Oceanography, 33(3):161–200. **https://doi.org/10.1016/0079-6611(94)90027-2**

Rahmstorf, S., 2006. Thermohaline ocean circulation. In Elias, S.A., Encyclopedia of Quaternary Sciences. Amsterdam (Elsevier), 739–750.

Riaza, C., and Martínez Del Olmo, W., 1996. Depositional model of the Guadalquivir – Gulf of Cadiz Tertiary basin. In Friend, P.F. and Dabrio, C.J., Tertiary Basins of Spain: The Stratigraphic Record of Crustal Kinematics. Cambridge (Cambridge University Press), 330–338. **https://doi.org/10.1017/CBO9780511524851.047**

Rodrigues, S., Roque, C., Hernández-Molina, F.J., Llave, E., and Terrinha, P., 2020. The sines contourite depositional system along the SW Portuguese margin: Onset, evolution and conceptual implications. Marine Geology, 430:106357. **https://doi.org/10.1016/j.margeo.2020.106357**

Rogerson, M., Bigg, G.R., Rohling, E.J., and Ramirez, J., 2012a. Vertical density gradient in the eastern North Atlantic during the last 30,000 years. Climate Dynamics, 39(3):589–598. **https://doi.org/10.1007/s00382-011-1148-4**

Rogerson, M., Colmenero-Hidalgo, E., Levine, R.C., Rohling, E.J., Voelker, A.H.L., Bigg, G.R., Schönfeld, J., Cacho, I., Sierro, F.J., Löwemark, L., Reguera, M.I., de Abreu, L., and Garrick, K., 2010. Enhanced Mediterranean-Atlantic exchange during Atlantic freshening phases. Geochemistry, Geophysics, Geosystems, 11(8):Q08013. **https://doi.org/10.1029/2009GC002931**

Rogerson, M., Rohling, E.J., Bigg, G.R., and Ramirez, J., 2012b. Paleoceanography of the Atlantic-Mediterranean exchange: overview and first quantitative assessment of climatic forcing. Reviews of Geophysics, 50(2):RG2003. **https://doi.org/10.1029/2011RG000376**

Rogerson, M., Rohling, E.J., and Weaver, P.P.E., 2006. Promotion of meridional overturning by Mediterranean-derived salt during the last deglaciation. Paleoceanography, 21(4):PA4101. **https://doi.org/10.1029/2006PA001306**

Rohling, E.J., 2007. Progress in paleosalinity: overview and presentation of a new approach. Paleoceanography, 22(3):PA3215. **https://doi.org/10.1029/2007PA001437**

Rouchy, J.M., Caruso, A., Pierre, C., Blanc-Valleron, M.-M., and Bassetti, M.A., 2007. The end of the Messinian salinity crisis: evidences from the Chelif Basin (Algeria). Palaeogeography, Palaeoclimatology, Palaeoecology, 254(3):386–417. **https://doi.org/10.1016/j.palaeo.2007.06.015**

Roveri, M., Flecker, R., Krijgsman, W., Lofi, J., Lugli, S., Manzi, V., Sierro, F.J., Bertini, A., Camerlenghi, A., De Lange, G., Govers, R., Hilgen, F.J., Hübscher, C., Meijer, P.T., and Stoica, M., 2014. The Messinian salinity crisis: past and future of a great challenge for marine sciences. Marine Geology, 352:25–58. **https://doi.org/10.1016/j.margeo.2014.02.002**

Ryan, W.B.F., Hsü, K.J., et al., 1973. Initial Reports of the Deep Sea Drilling Project, 13: Washington, DC (US Government Printing Office). **https://doi.org/10.2973/dsdp.proc.13.1973**

Schimmelmann, A., Lange, C.B., Schieber, J., Francus, P., Ojala, A.E.K., and Zolitschka, B., 2016. Varves in marine sediments: A review. Earth-Science Reviews, 159:215–246. **https://doi.org/10.1016/j.earscirev.2016.04.009**

Siegenthaler, U., and Sarmiento, J.L., 1993. Atmospheric carbon dioxide and the ocean. Nature, 365(6442):119–125. **https://doi.org/10.1038/365119a0**

Sierro, F.J., Delgado, J.A.G., Dabrio, C.J., Flores, J.A., and Civis, J., 1996. Late Neogene depositional sequences in the foreland basin of Guadalquivir (SW Spain). In Friend, P.F. and Dabrio, C.J., Tertiary Basins of Spain: The Stratigraphic Record of Crustal Kinematics. Cambridge (Cambridge University Press), 339–345. **https://doi.org/10.1017/CBO9780511524851.048**

Smethie, W.M., Jr., Fine, R.A., Putzka, A., and Jones, E.P., 2000. Tracing the flow of North Atlantic Deep Water using chlorofluorocarbons. Journal of Geophysical Research: Oceans, 105(C6):14297–14323. **https://doi.org/10.1029/1999JC900274**

Smith, A.G., and Pickering, K.T., 2003. Oceanic gateways as a critical factor to initiate icehouse Earth. Journal of the Geological Society, 160(3):337–340. **https://doi.org/10.1144/0016-764902-115**

Stow, D.A.V., and Faugères, J.C., 2008. Contourite facies and the facies model. In Rebesco, M., and Camerlenghi, A. (Eds.), Contourites. Developments in Sedimentology, 60: (Elsevier), 223–256. **https://doi.org/10.1016/S0070-4571(08)10013-9**

Suárez Alba, J., Martínez del Olmo, W., Serrano Oñate, A., and Leret Verdú, G., 1989. Estructura del sistema turbidítico de la Formación Arenas del Guadalquivir. In Libro homenaje a Rafael Soler y José. Madrid (Asociación de Geólogos y Geofísicos Españoles del Petróleo), 123–136.

Sykes, T.J.S., Ramsay, A.T.S., and Kidd, R.B., 1998. Southern hemisphere Miocene bottom-water circulation: a palaeobathymetric analysis. Geological Society, London, Special Publications, 131(1):43–54. **https://doi.org/10.1144/GSL.SP.1998.131.01.03**

Tans, P.P., Berry, J.A., and Keeling, R.F., 1993. Oceanic $^{13}C/^{12}C$ observations: a new window on ocean CO_2 uptake. Global Biogeochemical Cycles, 7(2):353–368. **https://doi.org/10.1029/93GB00053**

Taylforth, J.E., McCay, G.A., Ellam, R., Raffi, I., Kroon, D., and Robertson, A.H.F., 2014. Middle Miocene (Langhian) sapropel formation in the easternmost Mediterranean deep-water basin: evidence from northern Cyprus. Marine and Petroleum Geology, 57:521–536. **https://doi.org/10.1016/j.marpetgeo.2014.04.015**

Thomas, H., Bozec, Y., Elkalay, K., and de Baar, H.J.W., 2004. Enhanced open ocean storage of CO_2 from shelf sea pumping. Science, 304(5673):1005–1008. **https://doi.org/10.1126/science.1095491**

Uenzelmann-Neben, G., Weber, T., Grützner, J., and Thomas, M., 2017. Transition from the Cretaceous ocean to Cenozoic circulation in the western South Atlantic — a twofold reconstruction. Tectonophysics, 716:225–240. **https://doi.org/10.1016/j.tecto.2016.05.036**

van Aken, H.M., 2000. The hydrography of the mid-latitude northeast Atlantic Ocean: I: The deep water masses. Deep Sea Research Part I: Oceanographic Research Papers, 47(5):757–788. **https://doi.org/10.1016/S0967-0637(99)00092-8** van der Schee, M., Sierro, F.J., Jiménez-Espejo, F.J., Hernández-Molina, F.J., Flecker, R., Flores, J.A., Acton, G., Gutjahr, M., Grunert, P., Garcia-Gallardo, A., and Andersen, N., 2016. Evidence of early bottom water current flow after the Messinian Salinity Crisis in the Gulf of Cadiz. Marine Geology, 380:315–329. **https://doi.org/10.1016/j.margeo.2016.04.005**

van Hinsbergen, D.J.J., Vissers, R.L.M., and Spakman, W., 2014. Origin and consequences of western Mediterranean subduction, rollback, and slab segmentation. Tectonics, 33(4):393–419. **https://doi.org/10.1002/2013TC003349**

Voelker, A.H.L., Lebreiro, S.M., Schönfeld, J., Cacho, I., Erlenkeuser, H., and Abrantes, F., 2006. Mediterranean outflow strengthening during northern hemisphere coolings: a salt source for the glacial Atlantic? Earth and Planetary Science Letters, 245(1):39–55. **https://doi.org/10.1016/j.epsl.2006.03.014**